galaxies

MDPI

Review

Radio Galaxies at TeV Energies

Cameron Rulten

Centre for Advanced Instrumentation, Department of Physics, University of Durham, South Road, Durham DH1 3LE, UK; cameron.b.rulten@durham.ac.uk

Abstract: Unlike blazars, radio galaxies have jets that are misaligned relative to our line-of-sight. This misaligned geometry provides us with a unique view of both the jet and super massive black hole. To date, four radio galaxies have been detected at TeV energies with an additional two active galactic nuclei shown to exhibit both radio galaxy and BL Lac-type properties. TeV observations of radio galaxies have revealed these objects to be fascinating, displaying ultra-fast variability and often relatively hard spectral energy distributions. This work aims to provide a review of the current state of radio galaxy observations within the context of very-high-energy γ-ray astronomy, while also highlighting that radio galaxies are excellent targets for multi-wavelength observations. A number of motivations for the continued study of radio galaxies are provided, and these are discussed with a focus on the key observational results, including implications for future observations with next-generation instruments soon to be operational.

Keywords: radio galaxies; active galactic nuclei; gamma-rays; non-thermal; jets

check for updates

Citation: Rulten, C. Radio Galaxies at TeV Energies. *Galaxies* **2022**, *10*, 61. https://doi.org/10.3390/galaxies10030061

Academic Editors: Phil Edwards and Yosuke Mizuno

Received: 15 February 2022
Accepted: 14 April 2022
Published: 22 April 2022

Publisher's Note: MDPI stays neutral with regard to jurisdictional claims in published maps and institutional affiliations.

1. Introduction

Active Galactic Nuclei (AGNs) can be defined as the compact regions at the centre of a galaxy in the process of accreting gas through a disk onto the supermassive black holes (SMBHs) residing at their cores. Detected across a broad band of electromagnetic frequencies/wavelengths, AGNs are typically characterised by their high non-stellar luminosity, and these objects can form jets of plasma extending outward from their SMBHs. Strong radio emission from a small fraction of AGNs indicates the presence of a relativistic jet [1], but it is still unknown as to why only some fraction of AGNs produce jets, while others do not. It is believed that a few AGN properties—mass, spin, accretion rate and mode, and spin orientation—along with the environment, determine whether an AGN is jetted or not, but a clear consensus is still to be reached [2–7].

Radio galaxies are a subclass of AGNs that are powerful emitters of radio waves, delivering approximately a million times more power ($\sim 10^{38}$ watts) than our own Milky Way Galaxy ($\sim 10^{32}$ watts). Typically, radio galaxies are characterised as having a bright compact core that is coincident with the visible nucleus of the galaxy. However, the radio emission extends beyond this core along jets that propagate outward from the central core to distances of pc or even kpc scales, as seen in NGC 6251 for example [8]. At the termination site of these jets, large plumes are often visible far beyond the central confines of the core. For a comprehensive discussion of relativistic jets from AGNs, which is beyond the scope of this work, please see the excellent review by [9] and all the references therein.

A large number of radio-loud AGN sub-classes are defined based on observational properties seen in specific wavebands, and it is suggested that radio galaxies form the parent population of blazars (AGNs with a relativistic jet pointing toward us). The radio galaxies with an edge-darkened morphology known as FR-Is (Fanaroff and Riley classification, [10]) correspond to BL Lacs observed at large jet viewing angles, while edge-brightened lobe morphology FR-II radio galaxies are associated with flat-spectrum radio quasars (FSRQs) [11]. The distinction between FR-I and FR-II radio galaxies is largely their radio power [12], where FR-Is are weaker, but more common and, hence, more likely to be

in a sample of nearby galaxies. Doppler boosting decreases as the jet viewing angle (i) to the line-of-sight increases. Therefore, within the context of VHE γ-ray astronomy, we refer to radio galaxies as radio-loud AGNs with jet viewing angles beyond the blazar condition ($i < 10^{\circ}$), yet the angle remains small enough for the detection of Doppler-boosted γ-rays. In practice, this includes objects falling near the boundary, and these may exhibit properties of both radio galaxies and blazars (but less extreme). While this distinction between blazars and radio galaxies is somewhat arbitrary, due to relativistic effects and strong Doppler boosting along the line-of-sight, blazars may exhibit features (such as Doppler factors > 10 and apparent speeds $> 10\,c$ [13]) that one would not expect to see in radio galaxies. A review of blazar characteristics is beyond the scope of this work; instead, the reader is directed to the following references [14–16] also within this Special Edition publication of the *Galaxies* journal.

To date, four radio galaxies (all of them FR-Is) have been detected at TeV energies using ground-based imaging atmospheric Cherenkov telescopes (IACTs) such as the High Energy Stereoscopic System (H.E.S.S.) [17], the Major Atmospheric Gamma Imaging Cherenkov Telescopes (MAGIC) [18,19], and the Very Energetic Radiation Imaging Telescope Array System (VERITAS) [20,21]. Of the 84 AGNs detected at TeV energies, all but 6 are blazars. Of these, the four detected radio galaxies are: M 87, Cen A, NGC 1275, and 3C 264. The other two AGNs (PKS 0625-35 and IC 310) show both radio galaxy and blazar properties [22]. In addition to the extragalactic sources highlighted above, IACTs have also detected two starburst galaxies, M 82 [23] and NGC 253 [24]. Unlike the AGN-powered radio galaxies and blazars, these extragalactic objects are characterised by their high star-formation rate, where gamma-ray emission is believed to originate from the acceleration of cosmic rays within the numerous shock waves caused by the high abundance of supernova remnants around massive young stars.

Over the past decade or so, γ-ray astronomy has seen considerable advances. This results from two critical factors: improved analysis techniques for IACTs to extract the maximum information from their data and the existence of the Large Area Telescope aboard NASA's *Fermi* satellite (*Fermi*-LAT) [25]. The situation is set to improve further at very high energies (VHE) with the advent of the Cherenkov Telescope Array (CTA) [26], providing coverage from a few 10s of GeV to several hundred TeV with unprecedented sensitivity. Seamless coverage of the electromagnetic spectrum spanning eight orders of magnitude in energy is now within our grasp.

Furthermore, as Meyer et al. [27] reported, observation baselines on the order of 20 years for the Hubble Space Telescope (HST) [28–30] and 40 years for the Very Large Array (VLA) [31,32], coupled with major advances in astrometry techniques, have led to great improvements in our understanding of jet kinematics. Additionally, with very-large-baseline interferometry (VLBI) [33] observations, we have seen superluminal proper motions (discovered for example in the quasars 3C 279 and 3C 273 [34]) within the inner regions of extragalactic jets, but how jet velocities evolve from these parsec scales to kiloparsec (and beyond) scales is still something of a mystery. Understanding how these jets evolve along their paths toward interacting with the intergalactic medium is critical for our understanding of jet structures and how much of the energy budget jets are able of carrying and depositing out in the AGN's large-scale environment. Meyer et al. [27] also reported that by pairing long-time-baseline observations of the kpc-scale jets with HST (capable of achieving accuracies for proper motion measurements of a tenth of a milliarcsecond per year), with VLA and with VLBI measurements of the parsec-scale jet, astronomers are now able to map the full velocity profile of jets from close to their SMBHs to beyond the extents of their host galaxy. Furthermore, with new radio and optical instruments coming online soon, all of which should be operational concurrently with CTA, the accuracy and extent to which we can measure the proper motions of extragalactic jets is expected to improve further still.

The aim of this work is to review the current state of radio galaxies relating to VHE γ-ray astronomy. Focus is placed on the four TeV-detected AGNs often classified as FR-Is,

and for the purpose of this review, these are referred to as radio galaxies (in line with the convention of the VHE community), even though these AGNs may be close to the boundary with blazars. For an earlier review of radio galaxies addressing TeV challenges, please see [35]. Section 2 provides some context by introducing some key characteristics of radio galaxies in terms of blazar studies and long-term γ-ray observations at GeV energies, as well as highlighting some motivations for the continued study of radio galaxies at VHE. Section 3 focuses on the results and findings from observations of radio galaxies detected at VHE, while finally, Section 4 discusses the implications of these key results, as well as addressing some of the future opportunities relating to the observation of radio galaxies with the next-generation of radio and TeV γ-ray observatories.

2. Radio Galaxies in Context

2.1. Blazar Studies

Understanding how jets are formed, collimated, and accelerated to relativistic speeds is a key goal of blazar studies. The jet emission from blazars and radio galaxies is characterized by a double-peaked, non-thermal spectral energy distribution (SED) [36]. The lower-frequency peak, which in blazars has a peak frequency ranging from 10^{12} to 10^{18} Hz, is well described as synchrotron emission. The higher-frequency peak (10^{18} Hz–10^{27} Hz) is generally attributed to inverse-Compton (IC) emission arising from synchrotron self-Compton (SSC) [37–39] or external Compton (EC) processes[1], or a combination of the two. Typically, the sources with higher-frequency synchrotron peaks have IC peaks in the ∼10–100 GeV energy range. Thus, high-synchrotron-peak (HSP) blazars ($\nu_{peak} > 10^{15}$ Hz) are the brightest and best-studied at VHE (currently, 53 of the AGNs detected at VHE), although they are the least powerful. Only nine blazars in the current TeV catalogue are low-synchrotron-peak (LSP) objects ($\nu_{peak} \leqslant 10^{14}$ Hz), including both FSRQs and BL Lacs.

Unlike blazars, radio galaxy jets are thought to be oriented at larger angles to the line-of-sight ($\geqslant 10^{\circ}$), implying they are are much less Doppler-boosted than blazars, thus exhibiting SEDs similar to LSP blazars [40]. There does appear to be an observed relationship between jet and accretion power [41]. It is also postulated that, in addition to differentiating source classes by accretion modes, a range of jet viewing angles is needed to explain a blazar sequence; low-power jets with inefficient accretion have structured jets [42], whereby the synchrotron peak frequency decreases as the "misalignment" increases and observations probe the lower-speed sheath of the jet. In this scenario, radio galaxies should then cluster at the low end of the synchrotron peak frequency distribution [40].

Keenan et al. [43] extended this idea, with a resulting catalogue of over 2000 radio-loud AGNs with well-sampled synchrotron SEDs (including over 1000 with jet power estimates) showing the distribution of sources on the synchrotron peak—luminosity (L) peak plane is driven by a dichotomy in jet strength where weak jet sources associated with inefficient accretion dominate at $\log(\nu_{peak}) > 15$ and strong jet sources with efficient accretion are primarily found with $\log(L_{peak}) > 45$ and $\log(\nu_{peak}) < 15$. This shows that the blazar sequence is at least in part due to a selection effect.

2.2. Radio Galaxies at GeV Energies

Over the past decade, *Fermi*-LAT has provided a high-quality view of the γ-ray sky at GeV energies, detecting a number of radio galaxies during the course of its mission. These observations have acted as a pathfinder for TeV observations, for using the current generation of ground-based IACTs, as well as for predicting future observations with CTA, e.g., [44]. In the recently released incremental version of the fourth *Fermi*-LAT point-source catalogue, which covers the first 12 years of the *Fermi*-LAT mission (4FGL-DR3) [45], there are a total of 43 non-blazar AGN classified as radio galaxies. The 4FGL-DR3 details for these radio galaxies are highlighted in Tables 1 and 2. Table 1 shows the radio galaxies that have *Fermi*-LAT-recorded SEDs best fitted with a power-law model, whereas Table 2 shows the radio galaxies that have *Fermi*-LAT-recorded SEDs best fitted with a log-parabola model.

Table 1. The *Fermi*-LAT 4FGL-DR3 radio galaxies, sorted by right ascension, that exhibit SEDs best fitted with a power-law model. Although Cen A is listed in this table, its SED is actually best fitted with a broken power-law model, as discussed in this review and elsewhere, e.g., [46,47]. The columns include the 4FGL catalogue name, an alternative object name, the type of model best fitted to the SED where PL is for power-law, the spectral index value (Γ), the photon flux between 1–100 GeV [photons cm^{-2} s^{-1}], the 4FGL-DR3 variability index where an index value >18.48 indicates a <1% chance of being a steady source, and a TeVCat flag indicating whether the object is detected at TeV energies.

4FGL Name	Object	Model	Γ	$F_{E=1-100\,GeV}$	Variability	TeVCat
4FGL J0009.7-3217	IC 1531	PL	2.24	2.02×10^{-10}	27.9362	N
4FGL J0038.7-0204	3C 17	PL	2.84	1.77×10^{-10}	17.5947	N
4FGL J0057.7+3023	NGC 315	PL	2.38	2.74×10^{-10}	8.81993	N
4FGL J0153.4+7114	TXS 0149+710	PL	1.93	2.60×10^{-10}	13.9387	N
4FGL J0237.7+0206	PKS 0235+017	PL	2.10	1.36×10^{-10}	6.75128	N
4FGL J0308.4+0407	NGC 1218	PL	2.00	8.44×10^{-10}	37.8178	N
4FGL J0312.9+4119	B3 0309+411B	PL	2.49	1.74×10^{-10}	21.8156	N
4FGL J0316.8+4120	IC 310	PL	1.85	2.52×10^{-10}	31.8913	Y
4FGL J0322.6-3712e	Fornax A	PL	2.05	5.59×10^{-10}	14.2643	N
4FGL J0334.3+3920	4C +39.12	PL	1.85	2.14×10^{-10}	14.2155	N
4FGL J0519.6-4544	Pictor A	PL	2.54	2.95×10^{-10}	11.9384	N
4FGL J0627.0-3529	PKS 0625-35	PL	1.91	1.26×10^{-09}	25.0043	Y
4FGL J0708.9+4839	NGC 2329	PL	1.72	1.04×10^{-10}	13.1158	N
4FGL J0758.7+3746	NGC 2484	PL	2.23	1.39×10^{-10}	7.38446	N
4FGL J0931.9+6737	NGC 2892	PL	2.28	4.75×10^{-10}	49.7003	N
4FGL J0958.3-2656	NGC 3078	PL	2.16	1.68×10^{-10}	7.16341	N
4FGL J1116.6+2915	B2 1113+29	PL	1.61	3.54×10^{-11}	11.7614	N
4FGL J1144.9+1937	3C 264	PL	2.02	2.95×10^{-10}	5.42454	Y
4FGL J1149.0+5924	NGC 3894	PL	2.19	2.20×10^{-10}	10.8819	N
4FGL J1219.6+0550	NGC 4261	PL	2.09	1.83×10^{-10}	13.2929	N
4FGL J1236.9-7232	PKS 1234-723	PL	2.40	2.34×10^{-10}	6.54389	N
4FGL J1306.3+1113	TXS 1303+114	PL	1.86	1.37×10^{-10}	14.3789	N
4FGL J1325.5-4300	Cen A	PL	2.59	3.59×10^{-09}	33.403	Y
4FGL J1443.1+5201	3C 303	PL	2.15	1.59×10^{-10}	9.88656	N
4FGL J1449.5+2746	B2 1447+27	PL	1.46	5.24×10^{-11}	12.7277	N
4FGL J1516.5+0015	PKS 1514+00	PL	2.51	3.03×10^{-10}	16.249	N
4FGL J1518.6+0614	TXS 1516+064	PL	1.79	1.10×10^{-10}	6.96701	N
4FGL J1521.1+0421	PKS B1518+045	PL	2.04	1.26×10^{-10}	21.5818	N
4FGL J1530.3+2709	LEDA 55267	PL	2.01	8.30×10^{-11}	12.2306	N
4FGL J1724.2-6501	NGC 6328	PL	2.56	1.87×10^{-10}	6.27477	N
4FGL J1843.4-4835	PKS 1839-48	PL	2.03	1.46×10^{-10}	4.58083	N
4FGL J2227.9-3031	PKS 2225-308	PL	1.80	1.11×10^{-10}	17.3154	N
4FGL J2302.8-1841	PKS 2300-18	PL	2.26	2.00×10^{-10}	14.3889	N
4FGL J2326.9-0201	PKS 2324-02	PL	2.59	2.27×10^{-10}	17.579	N
4FGL J2329.7-2118	PKS 2327-215	PL	2.45	4.00×10^{-10}	18.1362	N
4FGL J2341.8-2917	PKS 2338-295	PL	2.24	1.74×10^{-10}	13.6434	N

The photon indices of the 4FGL-DR3 radio galaxies best fitted with a power-law model are found to be in the range between 1.4 and 2.9. In addition, the photon fluxes of all the radio galaxies at GeV energies vary between $\sim 10^{-11}$ photons cm^{-2} s^{-1} and $\sim 10^{-8}$ photons cm^{-2} s^{-1}. As can be seen in Tables 1 and 2, the majority of *Fermi*-LAT-detected radio galaxies have an SED adequately described by a simple power-law model, at least over a long time period such as the 12 years covered by the 4FGL-DR3 catalogue. As defined in the original release of the 4FGL eight-year point source catalogue [48], a source is considered to be variable over yearly binned timescales if its Variability Index (shown in Tables 1 and 2) is larger than 18.48. Based on this measure, ∼72% of the *Fermi*-LAT radio galaxies are not considered variable and ∼28% are, with NGC 1275 and 3C 120 displaying

the strongest variability of all the *Fermi*-LAT-detected radio galaxies. However, given that many of these radio galaxies are faint (i.e., weak) γ-ray sources, it cannot be concluded for certain that these objects are not variable, but rather that *Fermi*-LAT cannot measure their variability.

Table 2. The *Fermi*-LAT 4FGL-DR3 radio galaxies, sorted by right ascension, that exhibit SEDs best fitted with a log-parabola model. The columns include the 4FGL catalogue name, an alternative object name, the type of model best fitted to the SED where LP is for log-parabola, the log-parabola spectral index value (α), the log-parabola spectral curvature value (β), the photon flux between 1–100 GeV [photons cm^{-2} s^{-1}], the 4FGL-DR3 variability index where an index value >18.48 indicates a <1% chance of being a steady source, and a TeVCat flag indicating whether the object is detected at TeV energies.

4FGL Name	Object	Model	α	β	$F_{E=1-100\,GeV}$	Variability	TeVCat
4FGL J0319.8+4130	NGC 1275	LP	2.05	0.07	3.38×10^{-08}	5460.94	Y
4FGL J0418.2+3807	3C 111	LP	2.62	0.23	7.23×10^{-10}	40.5743	N
4FGL J0433.0+0522	3C 120	LP	2.63	0.21	7.77×10^{-10}	308.796	N
4FGL J1230.8+1223	M 87	LP	2.01	0.04	1.62×10^{-09}	23.8056	Y
4FGL J1306.7-2148	PKS 1304-215	LP	1.86	0.24	5.22×10^{-10}	16.9549	N
4FGL J1630.6+8234	NGC 6251	LP	2.25	0.12	1.26×10^{-09}	7.34	N
4FGL J2156.0-6942	PKS 2153-69	LP	2.47	0.48	1.41×10^{-10}	5.73628	N

2.3. Motivations for Studying Radio Galaxies at TeV Energies

Within the context of TeV γ-ray astronomy, radio galaxies are typically thought of as "misaligned" AGNs with much reduced Doppler boosting factors. The detection of these objects at TeV energies was therefore somewhat of a surprise and opened up many questions about the γ-ray emission processes, γ-ray emission sites, and our general understanding about the nature of these extragalactic objects. Observations of radio galaxies are not overwhelmed with very strong Doppler-boosted emission (as is the case with blazars), and instead, the misaligned geometry provides us with a unique view of the AGN's jet and SMBH. Despite the small sample size, the detection of γ-rays from radio galaxies provides a number of motivations for future observations and studying these objects further. The following is a small selection of the outstanding questions relating to radio galaxies at TeV energies:

- Do all TeV-detected radio galaxies exist in dense clumpy environments, for example? What role does the environment play in decelerating radio galaxy jets, for example, and does this interaction lead to γ-ray emission and/or γ-ray orphan flares? (See [49] and the references therein.)
- Do TeV-detected radio galaxies exhibit any common kinematic characteristics? How do radio galaxies accelerate particles in their jets, and can regions with different apparent velocity profiles (over all jet scales) be correlated with γ-ray emission? What mechanisms give rise to features in radio galaxy jets, e.g., internal shocks, and are these responsible for gamma-ray emission?
- Is it right to classify the TeV-detected radio galaxies as misaligned blazars, or are these objects simply blazar-like, with much smaller jet inclination angles to the line-of-sight than currently derived or assumed?
- In TeV-detected radio galaxies, where does gamma-ray emission occur? Is it close to the black hole in the inner-jet region or at kpc scales further down the jet? Are there multiple γ-ray emission sites and components, for example, both jet and large-scale emission from the up-scatter of external photons?
- Are TeV-detected radio galaxies best described by a singular leptonic, hadronic, or mixed emission model? Which process dominates?
- Are TeV-detected radio galaxies cosmic ray sources? If γ-ray emission from radio galaxies can be correlated with neutrino observations, can the population of as-yet-

undetected radio galaxies in our universe make a substantial contribution towards the cosmic ray background?

Section 4 attempts to address some of the themes covered in these questions, but in order to resolve any of them, it is important to state that TeV observations alone cannot fully answer all of these questions. Instead, multi-wavelength observations from radio to optical to γ-rays are all needed, and we live in an exciting time with many new large and improved observatories on the horizon, all capable of making major contributions toward a better understanding of AGN science. Taking into account unification considerations [50], there is a motivation to explore these objects deeper and with higher precision. For example, to construct better theoretical emission models for radio galaxies, there is a need for well-sampled broadband spectra of these objects in different states. In order to do this at the highest energies, deeper observations are required. In addition, TeV observations provide us with the best opportunity to probe the fastest variability at the highest energies, as this will enable us to gain a better understanding of the nature of these objects and tell us more about the location of gamma-ray emission sites, for example whether the observed gamma-ray emission originates close to the core or further down the jet. Furthermore, it is suggested that given radio galaxies are now detected at both GeV and TeV energies, their large population likely provides a significant contribution toward the cosmic rays that permeate our universe. Therefore, multi-messenger observations of radio galaxies may provide us with insights into their overall contribution toward the cosmic ray background.

3. Results

As already mentioned above, four radio galaxies have been detected with ground-based IACTs. The discovery of these objects with the current generation of TeV instruments is exciting as this paves the way for some promising observations with future IACTs to provide new insights into the mechanisms driving gamma-ray emission. In this section, we highlight the key findings from the observations of the four TeV-detected radio galaxies including the additional two non-blazar AGN that display both radio galaxy and blazar characteristics. Table 3 highlights the key characteristics of these objects.

Table 3. Highlighted here are the key characteristics of the 6 non-blazar AGNs detected at TeV energies. The table is sorted by redshift in ascending order. The column details are as follows: the common name given to the AGN (Name), an alternative name for the AGN (Alt. Name), redshift (z), the jet inclination angle to the line-of-sight (θ_i (degrees)), jet power ($P^{jet}_{1.4\,GHz}$ (W/Hz)), radio luminosity at 5 GHz ($L_{5\,GHz}$ (ergs/s)), synchrotron peak frequency (ν_{peak} (Hz)), VHE discovery date (dd_{VHE} (year-month)), and finally, a column containing references for each object (Refs.).

Name	Alt. Name	z	θ_i	$\log P^{jet}_{1.4GHz}$	L_{5GHz}	$\log \nu_{peak}$	dd_{VHE}	Refs.
Cen A	NGC 5128	0.0018	12°–45°	21.97	1.91×10^{40}	12.81	2009-03	[22,43,51,52]
M 87	3C 274	0.0042	13°–27°	23.27	5.83×10^{39}	9.5	2003-05	[22,43,52,53]
NGC 1275	3C 84	0.0175	30°–55°	-	1.39×10^{42}	13.39	2010-10	[22,54]
IC 310	B3 0313+411	0.0188	∼8°	-	9.94×10^{39}	∼17.0	2010-03	[22,55,56]
3C 264	NGC 3862	0.0216	∼50°	23.67	9.54×10^{40}	16.30	2018-03	[22,43,52,57,58]
PKS 0625-35	TXS 0625-354	0.0562	<53°	-	7.67×10^{41}	∼16.0	2015-07	[22,59,60]

3.1. NGC 1275

NGC 1275 (also commonly known as 3C 84) is the brightest cluster galaxy at the centre of the Perseus cluster of galaxies. It is located at ∼75 Mpc and was detected by both MAGIC [61] and VERITAS [62]. Radio observations of NGC 1275 show a sub-parsec-scale radio jet oriented between ∼30° and 60° with possible bending in the jet. Figure 1 shows NGC 1275 at 43 GHz (left panel) and 22 GHz (right panel) radio frequencies. Here, we see the sub-parsec-scale jet appears to have a complex structure and is dominated by two features[2]: the core (A0) and a knot (C2) [63]. There does not appear to be evidence of superluminal apparent speeds in the parsec-scale jet; indeed; C2 moves at subluminal

speeds of ∼0.2c relative to the core. The left panel of Figure 1 also highlights a number of other knots (C1...C8), but the one with the highest recorded proper motion is C6 at ∼0.36c. Knot C3 appears to move upstream, while knot C4 appears to be at a significantly different, yet stable position angle. Recent observations suggest the component C3 is a remnant of previous emission [49,64].

The knot C2 emerged following a radio outburst in 2005 located in the central 1pc region [65]. After this outburst, limb-brightening of the jet was discovered, indicating that the transverse structure of the jet had changed. This morphological change appears to have coincided with an increased γ-ray flux level at GeV energies [66,67]. Furthermore, the radio emission from knot C2 was significantly polarized, and there appeared to be a location change from southwest to southeast. It is suggested that this movement and enhanced polarization indicated that the jet jittered in an inhomogeneous ambient medium [68]. A ∼0.4 mas directional flip of the knot C2 was confirmed with radio observations taken in 2015 and 2016, providing the first evidence of jet interaction with the environment [49]. It is believed the jet of NGC 1275 interacted/collided with a compact dense cloud, which led to a year-long frustration of the jet before breaking out in 2018. Subsequently, the knot C2 continued to move southward until eventually becoming distorted and returning NGC 1275 to a darkened lobe morphology state [64].

The high-resolution radio observations shown in the right panel of Figure 1 provide evidence of a limb-brightened jet. The large intensity ratio between the bright outer layer and the dim central region can be explained by transverse velocity structures and supports γ-ray emission scenarios via spine–sheath-structured jet models [42,69]. Sub-arcsecond optical images of NGC 1275 reveal a possible recent merger event [70], which is interesting because galaxy mergers are postulated to be potential sources of cosmic rays, neutrinos, and γ-rays [71].

NGC 1275 exhibits significant flux variability with flux doubling times of around 10 h observed, suggesting γ-ray emission originates from a compact region. In its quiescent state, the spectral shape of NGC 1275, determined from MAGIC observations, appears to follow a log-parabola (or power-law with sub-exponential cut-off) with a somewhat steep spectral index of $\Gamma \sim -4.1$ and no excess γ-ray photons above ∼650 GeV detected. In January 2017, significant increases in the flux levels seen from NGC 1275 were reported by MAGIC (∼1.5-times the flux from the Crab Nebula) [72] and VERITAS (∼65% the flux from the Crab Nebula) [73]. Significant variability was observed in the day-to-day light curve of NGC 1275 with a fastest flux-doubling timescale of (611 ± 101) min. seen [74]. Such a flux-doubling timescale implies that the emission region responsible for VHE γ-rays is larger than the event horizon light crossing time, but it still represents a compact region of the jet as opposed to a large-scale emission zone.

From these MAGIC observations of NGC 1275 during a flaring state, the MAGIC Collaboration et al. [74] attempted to model the observed SED assuming a classical SSC leptonic scenario. However, this was not possible due to the very-fast-variability scale constraining the size of emission zone at one to two orders of magnitude below that typically used in the SSC scenario adopted by the authors. In attempting to model the γ-ray emission from NGC 1275 by assuming an SSC leptonic scenario, and as hinted elsewhere, a higher Doppler factor would be needed to circumvent absorption, thus necessitating a jet inclination angle (to the line-of-sight) that is at odds with the jet inclination angle determined from radio observations.

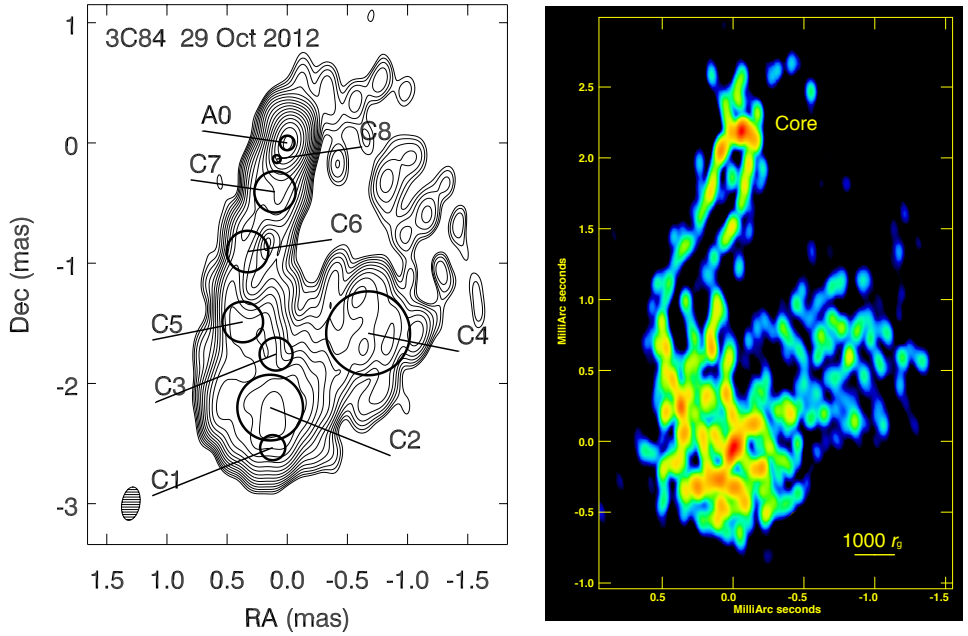

Figure 1. The **left** panel taken from [63] shows the total intensity image of NGC 1275 at 43 GHz radio frequencies. The parsec-scale jet shows a complex structure and is dominated by two features: the core (A0) and a knot (C2). Knot C6 has the highest recorded proper motion of ∼0.36c. The **right** panel taken from [67] shows the 22 GHz space-VLBI image of NGC 1275's jet from the core to ∼1pc. These high-resolution radio observations provide evidence of a limb-brightened jet. The large intensity ratio between the bright outer layer and the dim central region can be explained by transverse velocity structures and supports γ-ray emission scenarios via spine–sheath-structured jet models.

3.2. Cen A

Cen A (NGC 5128) is the nearest (d∼3.8 Mpc [75]) and one of the most well-studied extragalactic objects over a wide frequency domain. A misaligned FR-I radio galaxy, Cen A is often considered the prototypical Fanaroff–Riley FR-I classification. Cen A exhibits a complex and extended radio morphology with two giant lobes, as shown by the radio contours (black lines) in Figure 2. The latest sub-parsec-scale VLBI observations of Cen A obtained with the Event Horizon Telescope (EHT) at 228 GHz reveal a highly collimated, asymmetrically edge-brightened jet along with a faint counter-jet [76]. This strong limb-brightening seen in the sub-parsec-scale jet of Cen A is similar to that seen in other TeV-detected radio galaxies M 87 and NGC 1275, which suggests the dominant emission originates from the jet sheath and could potentially indicate that some component of γ-ray emission from Cen A takes place via spine–sheath-structured jet models.

Faint TeV γ-ray emission from Cen A was detected by H.E.S.S. after approximately ∼120 h of observations. The TeV emission was detected with a statistical significance of 5σ above the background coincident within a region including both the radio core and the inner kiloparsec jet. The integrated flux above ∼250 GeV was estimated to be ∼0.8% that of the flux from the Crab Nebula. A power-law shape was best fitted to the spectral energy distribution with a photon index of $2.7 \pm 0.5_{\mathrm{stat}} \pm 0.2_{\mathrm{sys}}$, and no significant flux variability was detected [77].

Using the first four years of *Fermi*-LAT data, Sahakyan et al. [46] first reported evidence (albeit not statistically significant at $< 3\sigma$) for an observed hardening of Cen A's energy spectrum. They reported a break in the spectrum at $E_b \sim 4$ GeV with a spectral index of $\Gamma_{E<4\,\mathrm{GeV}} = 2.74 \pm 0.03$ below and $\Gamma_{E>4\,\mathrm{GeV}} = 2.09 \pm 0.20$ above the break. Sahakyan et al. [46] suggested that the best-fitted broken power-law model could be caused by the contribution of an additional high-energy component beyond common synchrotron self-Compton jet emission. With eight years worth of *Fermi*-LAT data, Brown et al. [47] confirmed the existence of a statistically significant spectral hardening in Cen A's spectra,

a likelihood-ratio test with TS = 28.6 ≈ 5.3σ demonstrating that Cen A's spectra are best described by a broken power-law model compared to a standard power-law model. The spectral index values of their study agreed (within the reported errors) with those reported by Sahakyan et al. [46] both above and below the break energy. In addition, Brown et al. [47] found no evidence for significant flux variability from Cen A in either the low- or high-energy spectral components when considering the full eight-year dataset. However, they did note that their results showed some flux variability (at the 3.3σ level) in the low-energy spectral component during the first 3.5 years of *Fermi*-LAT data. The lack of variability, in particular for the high-energy spectral component, rules out the possibility that the spectral feature of Cen A is a result of jet-induced leptonic processes. Instead, Brown et al. [47] suggested that the feature seen in the combined GeV-TeV SED is consistent with a spike in the dark matter halo profile, but also postulated that a population of unresolved millisecond pulsars or some other population of energetic particles could be responsible for the spectral feature.

Single-zone SSC models do not adequately describe Cen A's observed broadband spectral energy distribution. As pointed out in [78], a variety of different scenarios exist, and none of them mutually exclusive, for the physical origin of the observed spectral energy break. To avoid going into great detail for each scenario here, the appropriate references are included again:

- Magnetospheric pulsar-like scenarios [79,80];
- Inner-jet models involving a number of leptonic SSC-emitting components that propagate at different angles relative to the line-of-sight [39], inverse-Compton emission from structured jets as discussed elsewhere in this article [42], photo-meson decay processes [81–84], lepto-hadronic emission models [85,86], and γ-ray-induced pair cascades from different regions [87–89];
- Extended emission scenarios such as the interaction of energetic protons with ambient matter (proton–proton interactions) at kiloparsec scales [46], millisecond pulsar contributions as already highlighted above [47], the inverse-Compton upscattering of photons on kiloparsec scales [90], or host galaxy starlight [91];
- The self-annihilation of dark matter, as already highlighted above [47].

With the current generation of IACTs, the jets of Cen A cannot be resolved. Therefore, distinguishing between these scenarios is currently difficult, and the observed γ-ray emission has tended to be associated with a region close to the black hole. Recent observations of Cen A by H.E.S.S. have focused on looking for extended emission and by comparing different models using a test statistic, and they found a strong preference for an elliptical Gaussian model (TS = 19.4) compared to a radially symmetric Gaussian model (TS = 6.1) [92]. This result, shown in Figure 2, implies that a major part of the VHE γ-ray emission originates on large scales at great distances from the SMBH.

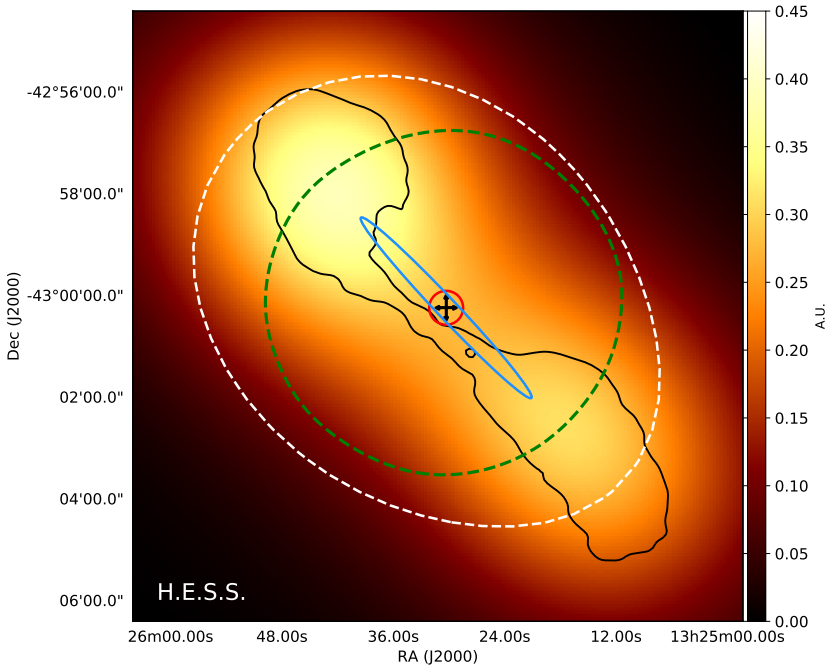

Figure 2. Taken from [92], the 21 cm VLA radio intensity map of Cen A after convolution with the H.E.S.S. point spread function (PSF) and additional oversampling (arbitrary units labelled as A.U.). The solid black lines show the unconvolved VLA radio contours for the inner lobes of Cen A. The white dashed line shows the VHE γ-ray morphology of Cen A derived from H.E.S.S. observations, and the best fit elliptical Gaussian is shown by the 1σ blue ellipse. The green dashed line shows the H.E.S.S. PSF 68% containment area.

3.3. M 87

M 87 (3C 274, NGC 4486) is a radio galaxy located in the Virgo cluster at a distance of $d \sim 16.7$ Mpc [93], making this the second closest radio galaxy after Cen A, but the closest kiloparsec-scale radio-optical jet. The jet of M 87 is misaligned with an angle $i \sim 15°$–$25°$ to the line-of-sight. M 87 is classified as a low-excitation weak-power FR-I-type radio galaxy displaying a radiatively inefficient accretion mode.

HST observations of M 87 provide evidence for superluminal speeds up to $\sim$6c out to $\sim$0.5 kpc [94], and radio observations of the feature known as HST-1 (located at a de-projected distance $>$ 100 pc) show superluminal speeds of $\sim$4c [95–97]. However, Kovalev et al. [98] found no evidence for motions faster than 0.07c within the inner $\sim$1.6 pc of the jet, and using radio images from the European VLBI Network, Asada et al. [99] suggested that the jet of M 87 is gradually accelerated from these subluminal speeds seen at the milliarcsecond scales of the inner-jet out to the superluminal speeds seen at HST-1. Mertens et al. [53] raised concerns with this scenario including the implied need for a jet-to-counter-jet intensity ratio of 1 when the jet of M 87 is essentially one-sided. Furthermore, the observed limb-brightened morphology of the jet strengthens the argument that the subluminal apparent speeds reported for the inner-jet point to a pattern speed or a wind from an outer sheath in the jet.

Using the 10 m Whipple Cherenkov telescope, in the years 2000/2001, early efforts were made by the VERITAS collaboration to detect VHE γ-ray emission from M 87 [100]. The question of whether M 87 emitted TeV γ-rays was again raised by Aharonian et al. [101] after finding excess photons (with a statistical significance of 4σ) at energies $E > 730$ GeV coincident with the position of the radio galaxy using data taken with HEGRA [102]. VHE γ-ray emission from M 87 was detected by H.E.S.S. with a statistical significance of 13σ [103] and thereby establishing M 87 as the first non-blazar extragalactic TeV source. In addition, the observations providing this first detection of M 87 at TeV energies also provided evidence for statistically significant spectral variability on the timescale of days. This early

detection strongly constrained the size of the γ-ray-emitting region and challenged most scenarios of VHE γ-ray production theorised at that time for extragalactic sources. The VERITAS collaboration also reported the detection of VHE γ-rays from M 87 showing a correlation between the VHE γ-ray flux and M 87's X-ray emission detected by the ASM RXTE observatory [104]. Observations by MAGIC also confirmed the detection of M 87 as a TeV source [105]. Again, these early observations seemed to suggest that the γ-ray emission was most likely associated with the core of the radio galaxy as opposed to a knot in the jet, for example. However, a detailed multi-wavelength study of M 87 by Abramowski et al. [106] showed two of three detected flares exhibited rapid variability, suggesting γ-ray emission close to the core and the remaining flare coincident with the brightening of an HST-1 knot in the jet. This study used both the historical VHE observations, as well as new VHE data obtained during several coordinated monitoring campaigns between 2008 and 2010.

Figure 3 shows a composite image of M 87 viewed across a broadband spectrum from radio to γ-ray frequencies. The image demonstrates the huge scales between images of the black hole at the heart of M 87 versus images encompassing the whole jet and extent of the radio galaxy itself. Figure 3 should also provide the reader with some insight into the challenges faced by astronomers when trying to understand and model the mechanisms driving the non-thermal emission from radio at one end of the electromagnetic spectrum to γ-rays at the other. Current instruments, at γ-ray energies, are not able to spatially resolve emission from the core and the jet.

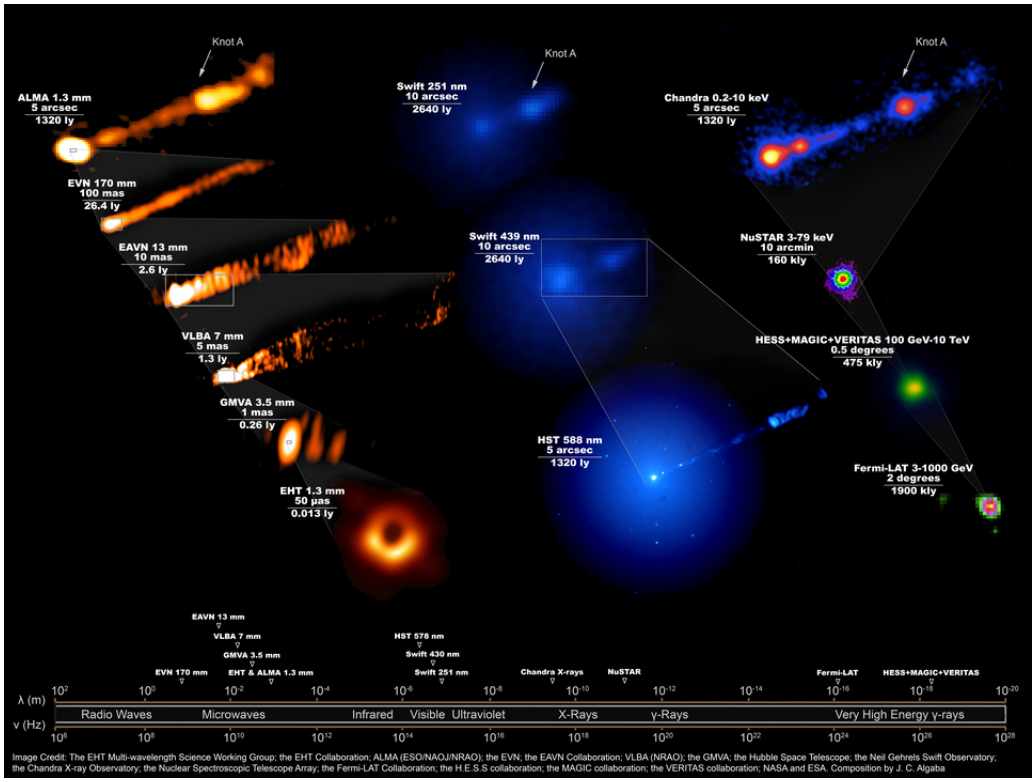

Figure 3. Taken from [107], a composite image of M 87 viewed across the broadband spectrum from radio frequencies to γ-ray frequencies. Shown here are the vast range of scales spanned by the AGN's black hole and its forward-pointing jet. Ground-breaking observations by the EHT has allowed us to image for the first time the SMBH at the heart of M 87. In addition, we can see various bright knots or features along the jet, for example Knot A clearly visible with ALMA, Swift, HST, and Chandra. Credit: the EHT Multi-Wavelength Science Working Group; the EHT Collaboration; ALMA (ESO/NAOJ/NRAO); the EVN; the EAVN Collaboration; VLBA (NRAO); the GMVA; the Hubble Space Telescope, the Neil Gehrels Swift Observatory; the Chandra X-ray Observatory; the Nuclear Spectroscopic Telescope Array; the Fermi-LAT Collaboration; the H.E.S.S. collaboration; the MAGIC collaboration; the VERITAS collaboration; NASA and ESA. Composition by J.C. Algaba.

3.4. 3C 264

The fourth radio galaxy detected at VHE energies is 3C 264. This was detected by VERITAS [20] between February 2017 and May 2019. At a distance of ∼93 Mpc, 3C 264 is the most distant radio galaxy detected at TeV energies, but is also one of the brightest and closest radio-optical jets known [108]. The excess γ-rays coincident with the location of 3C 264 were detected with a statistical significance of 7.8σ above the background. The detection of 3C 264 came from deep observations comprising some 57 h of data and is believed to have occurred during an elevated flux state during the 2018 observations [109]. Like M 87, 3C 264 exhibits superluminal motions on kiloparsec scales. When comparing the jet structure, 3C 264 closely resembles M 87. Both galaxies have one-sided FR-I-type jets with a kinetic luminosity of $\sim 10^{43.8}$ erg s^{-1} [40]. In addition, their jets display quite similar morphological traits, for example they both have multiple knots. Indeed, a one-to-one correspondence between radio and optical features was found in the jet of 3C 264 [110]. Like the other TeV-detected radio galaxies, 3C 264 exhibits a limb-brightened jet [111] indicating the possibility of γ-ray emission via spine–sheath-structured jet models. Using HST observations, Meyer et al. [112] found apparent speeds as high as $\beta_{\rm app} = (7.0 \pm 0.8)$c, exceeding the apparent speeds measured in the jet of M 87 highlighted in Section 3.3 above. Thus, 3C 264 could be considered as a more distant analogue of M 87, based on both its beamed and unbeamed radio emission, as well as its kinematic profile. 3C 264 is most likely observed at a smaller angle to the line-of-sight however.

The VHE flux observed by VERITAS during 2017–2019 shows slight variability, which suggests the detection did not result from a strong flare, but instead from a modestly enhanced flux state over a period of time. At GeV energies, 3C 264 shows some variability on six-monthly timescales, but compared to other *Fermi*-LAT-detected radio galaxies such as NGC 1275 or even 3C 120, it does not exhibit strong variability on these timescales [113]. At VHE energies, Archer et al. [109] reported 3C 264 showing variability on annual and monthly timescales. When comparing HST images of the jet in 3C 264 between 1994 and 2014, Meyer et al. [112] found two superluminal knots to be on a collision course. Indeed, the authors reported that these two knots began interacting during 2014 with the collision still ongoing today. Such an ongoing collision between two knots could be responsible for the observed VHE γ-ray emission. However, Archer et al. [109] concluded that the unresolved core was the most likely source of the enhanced VHE flux, particularly as there is no evidence for any notable changes in any of the contemporaneous high-resolution Chandra or HST images. The authors also stressed that no large changes in the core flux were seen at lower frequencies.

Figure 4 shows the broadband SED of 3C 264 compared to that of M 87. Archer et al. [109] were able to model the SED of 3C 264 successfully using a single-zone SSC model, although they did point out that a better fit could be achieved using a multi-zone model. However, from simple visual inspection, it is immediately noticeable that 3C 264 has a relatively high-frequency synchrotron peak near the X-ray frequency band ($\sim 10^{17}$ Hz), which appears to be somewhat unusual for a radio galaxy, as discussed in Section 2. In another study of 3C 264, the broadband SED and jet power were found to be reasonably well described by simple one-zone SSC leptonic models, but only when the high-energy component was associated with a second emitting region located at the end of the acceleration region (∼11 pc) in the spine or sheath of the jet. Furthermore, when the SED was modelled assuming synchrotron emission from the core, the emission at higher energies was significantly underpredicted [111].

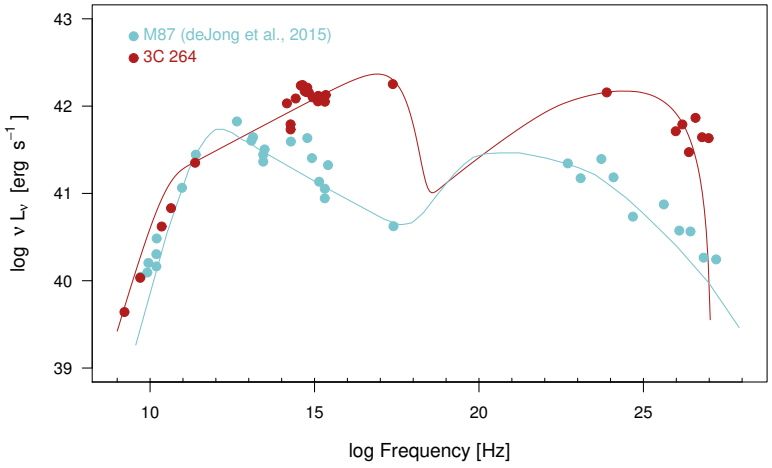

Figure 4. Taken from [109], a broadband SED for 3C 264 compared against that of M 87. Unlike the SED of M 87, which for a radio galaxy appears consistent with that expected according to the blazar sequence, the SED for 3C 264 shows a relatively high-frequency synchrotron peak near the X-ray frequency band ($\sim 10^{17}$ Hz).

3.5. PKS 0625-35 and IC 310

The two remaining non-blazar TeV-detected AGNs, PKS 0625-35 and IC 310, display both radio galaxy and blazar characteristics. TeV γ-rays (above an energy threshold of $\sim$250 GeV) from PKS 0625-35 were first detected in 2012 by H.E.S.S. with a statistical significance of $\sim 6\sigma$ above the background [114]. Located at a distance $d \approx 235$ Mpc ($z = 0.055$), PKS 0625-35 is much further away relative to other TeV-detected radio galaxies. Radio observations revealed a one-sided jet that extends to a distance of $\sim$143pc and exhibits superluminal apparent velocities of $\sim$3c [115–117]. Evidence for blazar characteristics was found in optical observations where the presence and intensity of the [OIII] emission line was consistent with those of other BL Lac objects [118]. In further work by the H. E. S. S. Collaboration et al. [119], it was suggested that PKS 0625-35 displays other unusual characteristics for a radio galaxy such as the synchrotron peak lying between ultraviolet and X-ray frequencies, which is typical for BL Lac objects. Furthermore, X-ray variability studies constrain the maximum possible misalignment to $\theta \approx 15^\circ$, and the authors therefore argued that the object be classified as a blazar or moderately misaligned blazar.

IC 310 is located in the Perseus cluster along with NGC 1275 and is at a distance of $d \approx 80$ Mpc ($z = 0.019$) from Earth. MAGIC made a serendipitous discovery of this head–tail radio galaxy during 2009/2010 while observing NGC 1275 located in the same field of view ($\sim 0.6^\circ$ away). An initial detection corresponding to a statistical significance of 7.6σ above the background was obtained from 20.6 h of stereoscopic observations [120,121]. The observed energy spectrum as seen by MAGIC was relatively hard with a spectral index $\Gamma = -2.00 \pm 0.14$. MAGIC estimated the average flux above 300 GeV to be $(3.1 \pm 0.5) \times 10^{-12}\,\mathrm{cm}^{-2}\,\mathrm{s}^{-1}$, which corresponds to $\sim$2.5% of the Crab Nebula flux [121]. An extensive multi-wavelength campaign observing IC 310 was conducted between 2012 and 2013. After data quality cuts, MAGIC acquired an additional $\sim$39 h on IC 310 including $\sim$3.7 h when MAGIC detected a bright flare. Thus, MAGIC was able to separate out this flare data to estimate energy spectra for two distinct states; during the low state, the energy spectrum is best described by a standard power-law model with normalisation at 1 TeV of $N_0 = (3.12 \pm 0.91) \times 10^{-13}\,\mathrm{TeV}^{-1}\,\mathrm{cm}^{-2}\,\mathrm{s}^{-1}$ and spectral index $\Gamma \approx (2.36 \pm 0.30)$, and during the bright flare, the energy spectrum reached a peak normalisation at 1 TeV of $N_0 = (44.2 \pm 2.1) \times 10^{-12}\,\mathrm{TeV}^{-1}\,\mathrm{cm}^{-2}\,\mathrm{s}^{-1}$ with spectral index $\Gamma \approx (1.51 \pm 0.06)$ [56].

Therefore, at TeV energies, the spectral index appears to display harder-when-brighter behaviour. Contemporaneous soft X-ray data taken during this multi-wavelength campaign appear to show a similar harder-when-brighter trend, and the authors concluded that this

relationship is consistent with an SSC emission scenario, successfully fitting a single-zone SSC model to the broadband SED during the non-flaring state. Similarly, at GeV energies, IC 310 appears highly variable in both flux and spectral state [122].

As mentioned above, the classification of IC 310 is still the subject of some debate. Originally classified as a narrow-angle tail (NAT) radio galaxy, early γ-ray detections of IC 310 categorized this object as an AGN of unknown type before being assigned as an HBL in the *Fermi*-LAT 2nd AGN catalogue. However, the discovery of a one-sided core–jet structure with blazar-like, beamed radio emission oriented along the kiloparsec tail was not consistent with the NAT classification. Instead, IC 310 appears to be a low-luminosity FR-I radio galaxy that is moderately misaligned i $\sim 10^{\circ}$–20° still revealing its BL Lac-type central engine [123]. Moreover, Figure 5 shows new low-frequency radio observations that provide a resolved view of the bent jets and have led to a new estimation of the misalignment to be i $\sim 8^{\circ}$. This evidence means that the γ-rays most likely originate from a small region close to the SMBH and are beamed toward us along the line-of-sight, within a region of the jet before it is bent into the narrow tail-like structure [55]. Furthermore, rapid minute-scale variability seen at TeV energies is consistent with such an interpretation.

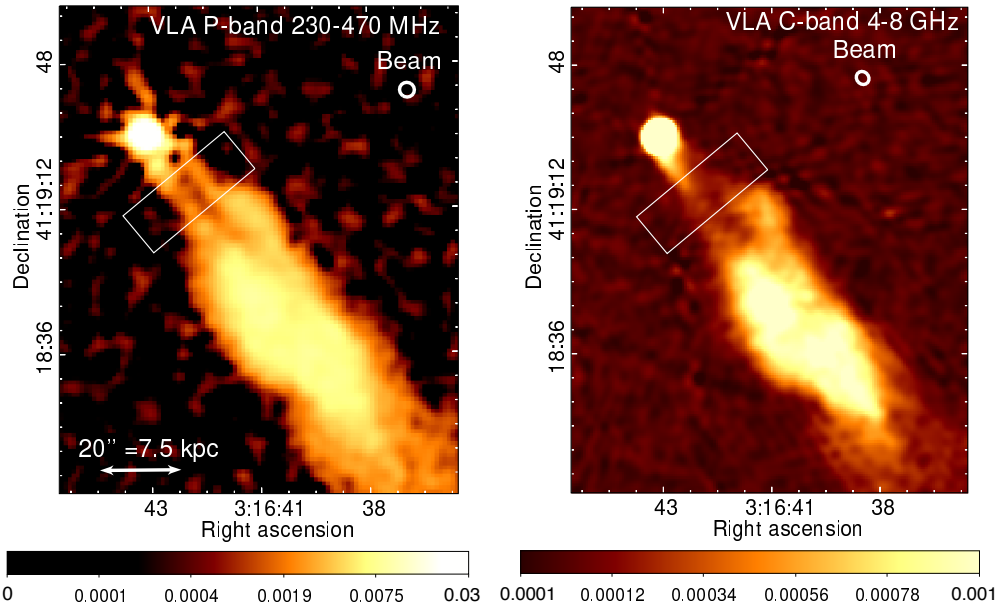

Figure 5. Taken from [55], these high-resolution VLA images of IC 310 show a zoomed-in region at the base of the jets. The left panel image from 320–470 MHz radio observations shows two distinct jets that are collimated, narrow, and oriented in the same general direction. The right panel image taken at higher radio frequencies of 4–8 GHz shows the same jet features, but closer to the nucleus, these are less distinguishable compared to the low-frequency observations. γ-ray emission most likely originates close to the SMBH in a region oriented close to our line-of-sight, where Doppler boosting takes place and before the jets are bent.

3.6. Radio Galaxies with Water Cherenkov Detectors

In addition to next-generation IACTs such as CTA, other techniques for exploring the VHE space, such as using water Cherenkov detectors (WCDs), were used in the past such as the VHE surveys conducted by Milagro [124,125] and ARGO [126]. At present, the High Altitude Water Cherenkov Observatory (HAWC) [127] located in central Mexico and a hybrid array called the Large High Altitude Air Shower Observatory (LHAASO) [128] in Sichuan province of China are operational, and another future observatory using WCDs called the Southern Wide-field Gamma-ray Observatory (SWGO) [129] (formerly the Southern Gamma-ray Survey Observatory) is also proposed. Observatories employing WCDs typically have a larger angular resolution compared to IACTs. However, compared to IACTs, their sensitivity for larger extended sources is better, and they are able to operate

both day and night under all weather conditions with a large instantaneous field of view > 2 sr. HAWC's angular resolution (defined as the 68% photon containment radius) is both energy- and zenith-angle-dependent and ranges from 0.1°–1° [127]. Furthermore, WCDs such as HAWC (and the proposed SWGO) are more sensitive to sources that transit directly overhead and also to sources with a hard energy spectrum. Thus, HAWC's energy threshold for detection is source-dependent. Naturally, this imposes a selection bias on the observable radio galaxies, but may be extremely useful in detecting any steady VHE γ-ray emission from radio galaxies, such as Cen A, that display spectral hardening in the GeV/TeV band and also display extended emission. Unfortunately, Cen A is not visible to HAWC, so undoubtedly will be a priority target for SWGO.

The relative closeness of radio galaxies means smaller γ-ray photon attenuation on the extragalactic background light (EBL), making these potentially great targets for studying the far-infrared band of the EBL above $\sim$10 TeV. In the latest results from the HAWC survey of active galaxies, six radio galaxies with favourable transits for HAWC were considered: NGC 1218, IC 310, NGC 1275, 4C +39.12, 3C 264, and M 87. At GeV energies, all of these radio galaxies have hard spectra; in the case of NGC 1275, this is true for active states. From live data spanning a period of approximately 4.5 years, HAWC sees only marginal evidence of γ-ray emission from M 87 with a statistical significance of $\sim 3.6\sigma$ at $E > 0.5$ TeV [130]. Similarly, M 87, NGC 1275, and IC 310 are all nearby sources within the LHAASO field of view [131], and since the observatory was only completed in 2021, observational findings for these sources will undoubtedly be published in the near future. Finally, even if WCDs require a longer integration time to reach the accepted statistical threshold to claim a detection, these types of detectors have a part to play in improving our understanding of radio galaxies, particularly if SWGO is able to bring advances that greatly improve the achievable angular resolution of current WCDs.

4. Discussion

The above sections have provided some context for radio galaxies within γ-ray astronomy by highlighting some key characteristics of these objects relating to wider blazar studies, as well as highlighting key findings from multi-wavelength observations of radio galaxies detected at VHE. This section will address some of the themes highlighted in Section 2.3 by discussing the principal findings from these observations and what implications if any these have for future observations of these fascinating extragalactic objects.

4.1. Radio Galaxy Environment

The first and probably most obvious finding from the TeV observations is that all four radio galaxies detected at VHE energies have low-power FR-I-type jets. This may seem counter-intuitive for accelerating particles to VHE, but equally, this may tell us that FR-I-type jets live in denser environments and that it is the interaction of the jet with these dense environments, rather than the intrinsic power of the jet, that provides the conditions for accelerating particles to VHE. For example, it is suggested that changes in the direction and flux of NGC 1275's bright C2 component (as shown in Figure 1) during August–September of 2015 are consistent with hydrodynamical simulations of jets in a clumpy ambient medium [49]. Furthermore, observations of 3C 264 show that the radio galaxy is located within a large region exhibiting low-surface-brightness emission, which could indicate that the radio galaxy resides in a dense environment [111]. Therefore, if radio monitoring reveals potential jet interactions/collisions with dense clumps in the environment (as in the case of NGC 1275 [49,64]), this could indicate an increased likelihood for enhanced γ-ray emission via internal shock models, leading to flares or possibly even orphan flares at TeV energies.

At the time of writing, no high-power FR-II-type radio galaxies are listed on TeVCat [22], but it is reasonable to assume that the current generation of ground-based IACTs have attempted to detect these objects without success. Perhaps this is not completely surprising given that FR-IIs are systematically farther away [132,133] and their VHE γ-ray

photons are more likely to be absorbed by the EBL, coupled with the fact that the current generation of IACTs simply does not possess the necessary sensitivity to detect γ-rays produced at their jet termination sites. If CTA is able to detect FR-II radio galaxies, this will expand our understanding of these objects further and provide better insight into the emission mechanisms at play, the emission locations, and perhaps, even their environments.

4.2. Kinematic Studies and Classification Considerations

Another obvious question one might ask is whether the TeV-detected radio galaxies are indeed radio galaxies in the "true sense", particularly as most of these objects exhibit properties such as a one-sided jet, fast variability, and superluminal motion, all characteristics of blazars, but less extreme in these cases. This of course is an argument of classification, and as already highlighted above, classification is often a product of the observed wavelength/frequency. Given that TeV emission from these extragalactic AGNs requires a relatively high Doppler factor, any blazars with jets not aligned closely to the line-of-sight are designated misaligned blazars. Thus, in the context of VHE γ-ray observations, this includes both "true" radio galaxies, as well as quasars, but also less extreme blazars falling near the radio galaxy boundary. There is no absolute angle used to precisely define the exact boundary of when a blazar becomes a radio galaxy; instead, if the jet is inclined with respect to the line-of-sight at angles $\theta \gtrsim 10^{\circ}$, then it is generally accepted that these are not BL Lacs, nor FSRQs in the strict sense. This corresponds to the critical angle used to distinguish the division between BL Lacs and FR-I-type radio galaxies [134].

In the case of IC 310, perhaps our understanding of the true nature of these objects is not complete. Perhaps γ-rays are emitted in regions that are closely aligned to our line-of-sight where large Doppler factors are attainable. What this result shows us is that high-resolution parsec- and kiloparsec-scale radio images are needed (in particular for radio galaxies that display rapid VHE variability) in order to better determine line-of-sight angles. Indeed, blazar multi-wavelength monitoring programs such as the MOJAVE survey program [135], the BEAM-ME program (successor to the VLBA-BU-BLAZAR program) [136], and the TANAMI program [59] are crucial as we enter a new era of observations with new instruments coming online soon, such as the James Webb Space Telescope (JWST) [137], the Square Kilometer Array (SKA) [138], and CTA [26], or planned, such as the Next-Generation Very Large Array (ngVLA) [139], as well as successors of Chandra [140] and *Fermi*-LAT.

Programs such as those highlighted above include many of the *Fermi*-LAT-detected radio galaxies and allow regular monitoring of radio amplitudes that enable correlation studies between radio and γ-ray frequencies. In addition, these monitoring programs can provide polarisation data that underline the magnetic field structure of the radio-emitting regions. All of this is crucial information that is needed when attempting to associate γ-ray emission with a particular region or emission process for example. Additionally, given the relatively poor angular resolution of γ-ray instruments, both from space and ground, very-long-baseline interferometry (VLBI) monitoring programs play a vital role in charting the evolution of parsec-scale radio emission, which again enables the study of any relationship between radio and γ-ray emission.

A further point for consideration is that we might only detect these four radio galaxies at TeV energies due to their proximity, i.e., even though they are misaligned, the combination of their proximity coupled with strong-enough Doppler boosting means they are detectable at TeV energies. However, it should be noted that at least two other *Fermi*-LAT-detected radio galaxies reside closer than 3C 264, and these are not detected at TeV energies. Furthermore, even though PKS 0625-35 displays blazar characteristics, it appears misaligned nonetheless, and there are many radio galaxies undetected at TeV energies closer than this object.

One last observation is that all four of the TeV-detected radio galaxies exhibit limb-brightened jets. Perhaps this is an important feature that could indicate an increased likelihood for gamma-ray emission via spine–sheath-structured jet models, where a small-enough beaming angle is maintained to provide sufficient Doppler boosting.

4.3. Emission Sites and Variability

The detection of synchrotron X-ray emission from the jets of Cen A and M 87 implies the presence of electrons at and above TeV energies, and it is possible that the TeV γ-ray emission is produced (or partly produced) by inverse-Compton scattering of photons by the high-energy electrons producing the synchrotron emission on kiloparsec scales [90]. Indeed, the detection of extended gamma-ray emission in Cen A with *Fermi*-LAT [141] coupled with a lack of evidence for strong variability means that an extended leptonic origin for its emission cannot be ruled out. As highlighted in Section 3.2, the latest H.E.S.S. observations of Cen A suggest that a major part of the VHE emission arises on large scales [92]. Moreover, the H.E.S.S. findings are consistent with (and provide the first evidence of) VHE γ-ray emission resulting from the inverse-Compton scattering of low-energy photons by ultra-relativistic electrons in the jet. This inverse-Compton emission potentially contributes toward the spectral hardening (discussed above) observed in Cen A and also suggests that radio galaxy jets are potentially a *steady* source of VHE gamma-rays.

However, in the case of M 87, the picture is not so clear. As highlighted above, two out of three TeV-detected flares exhibit rapid variability with timescales on the order of approximately half a day, which suggests that γ-ray emission originates from a region close to the core. Yet, the remaining TeV-detected flare was correlated (using multi-wavelength data) with the HST-1 knot located downstream in the jet of M 87 [106].

Fermi-LAT observations of M 87 found flux variability on six-monthly timescales at energies below $E < 10$ GeV [142]. Similarly, in a study of 26 radio galaxies at GeV energies using *Fermi*-LAT data [113], only 7 were seen to exhibit any statistically significant flux variability on six-monthly timescales. Of these seven, two (3C 264 and PKS 0625+35) were detected at TeV energies. On the other hand, NGC 1275 has displayed rapid variability at GeV energies during flares with flux-doubling timescales of 1.21 ± 0.22 h and 8.03 ± 1.24 h reported [143]. Such flux-doubling timescales are more usual for blazars rather than radio galaxies, but as already alluded to before, radio galaxies are weak γ-ray sources and the sensitivity of the current space- and ground-based γ-ray observatories limits us to seeing variability in the brightest radio galaxies.

4.4. Emission Mechanisms and Modelling

When modelling the broadband spectral energy distributions of blazars and indeed radio galaxies, often a single-zone synchrotron self-Compton (SSC) jet model is used to provide a reasonable description of the emission mechanisms. However, for radio galaxies such as Cen A with very modest Doppler boosting, it is clear that the single-zone SSC models do not adequately describe the VHE γ-ray emission [39,144,145]. Yet, for other radio galaxies such as 3C 264, its broadband emission spectrum can be described by a single-zone SSC model, as shown in Figure 4, but is probably better fit using multi-zone models [109].

When modelling the broadband SEDs of radio galaxies, the jet misalignment value used (or assumed) has a profound impact on the model used to describe the emission. Assuming TeV-detected radio galaxies displaying rapid variability are truly misaligned, then exotic scenarios such as "mini-jets in jets" [146] or "black-hole lightning" [147] are necessary in order to produce VHE γ-rays. In-depth discussion of all the models applicable to radio galaxies along with the intricacies of applying those models to SEDs is beyond the scope of this work. For a comprehensive review of blazar modelling in the context of TeV extragalactic astronomy please, see [16], and for an earlier review of radio galaxies at VHE energies that includes discussion of the models relevant to radio galaxies, please see [148]. Instead, what is important to take away is that radio galaxies are excellent targets for multi-wavelength observations, which provide us with an opportunity for correlation studies across wavebands in order to single out a preferred model (or set of models) that explain γ-ray emission from these objects.

4.5. Radio Galaxies as Cosmic Ray Sources

It is well established that cosmic ray particles permeating our galaxy cannot be traced back to their origins (except perhaps at the highest energies) as they are deflected by magnetic fields. We know that the origin of cosmic rays above a few EeV must be extragalactic, but as of yet, no specific type of source is positively identified as the primary cosmic ray contributor [149,150]. However, there is growing evidence in the Pierre Auger Observatory data (independent of the inconsistency arguments highlighted regarding the connection between ultra-high-energy cosmic rays (UHECRs) and AGNs) that Cen A is a potential source of UHECRs and neutrinos [150–154]. Indeed, the work by Koers and Tinyakov [155] highlights the possibility of Cen A being an exceptionally efficient neutrino source. This is important because if radio galaxies like Cen A are shown to be neutrino sources and can be correlated to TeV γ-ray emission in these objects, this provides very strong evidence that hadronic or lepto-hadronic emission processes are responsible.

Numerous authors have considered radio galaxies as candidates for neutrino events [156–159], and even FR-0-type radio galaxies were considered as well [160]. FR-0-type radio galaxies are a relatively new class of radio galaxy that display a different radio morphology to the observed FR-I- and FR-II-type radio galaxies. They lack the large-scale extended radio structures of the latter two classes, instead displaying jets that are both weak and short, extending only a few tens of kiloparsecs [161]. FR-0s share similar properties to those of FR-Is except the ratio of their core to total emission is $\sim$30-times higher than that of FR-I-type radio galaxies [162]. Despite the abundance of FR-0s in the local universe ($z < 0.05$), these are difficult objects to study because of their weak and compact nature [163]. No TeV emission is currently detected from an FR-0-type radio galaxy, but there are many open questions relating to these radio galaxies, not least the fact that at least one, 4C +39.12, was detected with *Fermi*-LAT at GeV energies displaying a relatively hard spectrum similar to that of 3C 264.

There is also evidence that a non-negligible positional association exists between AGNs with strong parsec-scale cores and neutrino events. This implies that AGNs with strongly Doppler-boosted jets, as opposed to radio galaxies, are an important source of neutrinos [164]. In spite of this, radio galaxies are important multi-messenger targets, in particular the closest radio galaxies Cen A and M 87.

As already discussed above, single-zone SSC models can be inadequate to explain the observed γ-ray emission from radio galaxies. The rising TeV components seen in the broadband SEDs of Cen A (and IC 310 during a flaring state) have led to suggestions of either a hadronic origin or leptonic origin with multiple electron distributions [47,165]. Using *Fermi*-LAT data, Rulten et al. [113] analysed 26 AGNs classified as radio galaxies in the *Fermi*-LAT 4FGL catalogue [48]. The goal of this work was to search for Cen A-like spectral features; no other radio galaxies exhibited a Cen A-like break in their spectral energy distributions. Whether other radio galaxies possess such a break is still an open question because, given *Fermi*-LAT's limited sensitivity at energies above 100 GeV coupled with the poor sensitivity of the current generation of IACTs for detecting weak γ-ray sources, the possibility still exists that other radio galaxies do indeed exhibit Cen A-like spectral breaks, but we just happen to see Cen A's because of the AGN's proximity to us. Discovery of such hardening amongst a greater number of radio galaxies would strongly implicate radio galaxies as a major source of cosmic rays within the universe.

4.6. Radio Galaxies with Future Instruments

It is imperative that TeV monitoring of radio galaxies continues, both with the current generation of IACTs, as well as with CTA when that instrument comes online. Deeper observations are necessary in order to better sample the energy spectra of these objects and, importantly, detect them in different states. Ideally, multi-wavelength campaigns should be run in order to capture data simultaneously, particularly important for correlating γ-ray emission with knots downstream in the jet. For example, a quasi-simultaneous multi-wavelength campaign monitoring M 87 produced the most comprehensive multi-

wavelength spectrum of the radio galaxy. Combining data from radio, optical, ultraviolet, X-ray, and gamma-ray wavebands, a near-complete broadband picture was produced during a historically low state for the AGN. In this work, the authors concluded that a structured jet is necessary to explain the observed spectrum of M 87 [166]. From modelling of the spectrum, the authors were able to exclude simultaneous γ-ray emission from inverse-Compton emission originating in the same region that produces the mm-band emission seen by the EHT. Moreover, the authors also concluded that γ-rays originating from the inner-jets (inward of HST-1) are only produced in the presence of strong particle-dominated regions [166]. However, they were not yet able to exclude direct synchrotron emission from accelerated protons (and secondaries). Such campaigns allow better modelling of radio galaxy broadband SEDs and provide the necessary information to favour a particular emission scenario for different AGN states.

Furthermore, the unequalled performance of CTA (relative to the current generation of IACTs) will allow γ-ray astronomers to investigate VHE emission from Cen A, for example with much better spatial and temporal resolution and sensitivity than ever before. Undoubtedly, this will help to better constrain the ratio of γ-ray emission between the core and extended regions of this particular radio galaxy.

New observatories such as SKA, JWST, and CTA will bring a new era of astronomy that will provide coverage of radio galaxies across the electromagnetic spectrum from radio to γ-ray frequencies, advancing our understanding of AGN physics. For example, at γ-ray energies, we know radio galaxies and blazars in general exhibit variability. The current generation of radio telescopes have limited survey speed, restricting the number of AGN with detailed variability studies to approximately a thousand of the brightest objects. Phase 1 of SKA will provide variability information at a sub-day-scale cadence for hundreds of thousands of AGN [167]. Such coverage will enable vastly improved multi-wavelength variability studies of radio galaxies between CTA and SKA, and perhaps facilitating the first insights into a radio-VHE connection, which has so far proven elusive. Furthermore, SKA is likely to play a crucial role in counterpart identification and classification of the many unidentified *Fermi*-LAT extragalactic γ-ray sources [168]. One of the most exciting discovery spaces in this new era regarding radio galaxies will perhaps come from the very-long-baseline interferometry (VLBI) capability of SKA complementing ngVLA advances, which is expected to provide ten-times the continuum imaging sensitivity of e-MERLIN [169] at 5 GHz in 1/10th the integration time, as well as achieving baselines of 1000 km [139]. Being able to conduct astrometry at the microarcsecond level out to tens of kiloparsecs will enable high-precision study of the proper motions of features inside radio galaxy jets [170]. Furthermore, with full linear and circular polarization capabilities, ngVLA will be able to study the magnetic field structure of radio galaxy lobes and hotspots with high precision, providing a better understanding of both the particle acceleration and jet deceleration and how this relates to γ-ray emission [139]. For example, do γ-ray flares occur after the radio emission peak and thus potentially indicating a jet "loading up" before emitting γ-rays, such as the creation of an emerging radio knot that interacts with an internal shock downstream in the jet [112]? Likewise, if no correlations are seen between γ-ray flares and knot brightening and the radio emission lags any γ-ray emission, this could be evidence that the primary γ-ray emission zone resides very close to the SMBH.

5. Conclusions

γ-ray observations of radio galaxies over the past decade or so have shown these objects to be fascinating, exhibiting ultra-fast variability or displaying relatively hard spectral energy distributions. These observations have also highlighted the need for instruments with improved sensitivity and resolution in order to better classify objects or to better resolve their morphological and timing characteristics, for example.

Although our understanding of radio galaxies as γ-ray emitters has advanced in the past decade or so, there still remains many outstanding questions, and a number of these were highlighted in Section 2.3. These relate to the radio galaxy environment, kinematic

studies, classification considerations, γ-ray emission sites, γ-ray variability, γ-ray emission mechanisms, γ-ray emission modelling, and radio galaxies as cosmic ray sources. From the discussion in Section 4, it is clear that many of these outstanding questions will need to be addressed with multi-wavelength studies, employing a number of different instruments.

Looking forward, the near-term horizon appears very promising with many new and improved instruments arriving, such as JWST, SKA, and CTA, to name a few. They will provide astronomers with many opportunities for future observations of radio galaxies. What is more, the unprecedented coverage and resolution of these instruments will help to advance our understanding of AGN science, for example by identifying γ-ray emission sites with better precision, by constructing high-quality apparent velocity profiles over all jet scales or through deeper observations with well-sampled broadband spectra to enable better modelling of γ-ray emission.

Funding: The author acknowledges the financial support of the UK Science and Technology Facilities Council Grant ST/V006347/1.

Institutional Review Board Statement: Not applicable

Informed Consent Statement: Not applicable

Data Availability Statement: Not applicable

Acknowledgments: The author would like to thank Professor Lucy Fortson (University of Minnesota) and Professor Paula Chadwick (University of Durham) for taking the time to read the article and provide valuable feedback and discussion, which has helped to improve the overall quality of the review. Finally, this research made use of the NASA/IPAC Extragalactic Database (NED), which is funded by the National Aeronautics and Space Administration and operated by the California Institute of Technology.

Conflicts of Interest: The author declares no conflict of interest.

Abbreviations

The following abbreviations are used in this manuscript:

AGNs	Active galactic nuclei
CTA	Cherenkov Telescope Array
EBL	Extragalactic background light
EHT	Event Horizon Telescope
FR-I	Fanaroff and Riley classification Type 1
FR-II	Fanaroff and Riley classification Type 2
FSRQ	Flat-spectrum radio quasar
GeV	Giga electron Volt
HAWC	High Altitude Water Cherenkov
H.E.S.S.	High Energy Stereoscopic System
HSP	High synchrotron peak
HST	Hubble Space Telescope
IACT	Imaging Atmospheric Cherenkov Telescope
IC	Inverse-Compton
JWST	James Webb Space Telescope
LSP	Low Synchrotron Peak
MAGIC	Major Atmospheric Gamma Imaging Cherenkov telescopes
ngVLA	Next-generation Very Large Array
PSF	Point spread function
SED	Spectral energy distribution
SKA	Square Kilometer Array
SMBH	Super massive black hole
SSC	Synchrotron self-Compton
TeV	Terra electron Volt
UHECR	Ultra-high-energy cosmic ray

VERITAS	Very Energetic Radiation Imaging Telescope Array System
VHE	Very high energy
VLA	Very Large Array
VLBI	Very-long-baseline interferometry
WCD	Water Cherenkov Detector

Notes

[1] In external Compton processes, the seed photons originate in regions external to the jet such as the accretion disk, the broad-line region, the AGN's dust torus, or molecular clouds, for example.

[2] In the literature, these two features are also referred to as C1 and C3, respectively, and under this alternative naming scheme, C4 (shown in Figure 1) is referred to as C2.

References

1. Wilson, A.S.; Colbert, E.J.M. The Difference between Radio-loud and Radio-quiet Active Galaxies. *Astrophys. J.* **1995**, *438*, 62. https://doi.org/10.1086/175054.
2. Tchekhovskoy, A.; Narayan, R.; McKinney, J.C. Black Hole Spin and The Radio Loud/Quiet Dichotomy of Active Galactic Nuclei. *Astrophys. J.* **2010**, *711*, 50–63. https://doi.org/10.1088/0004-637X/711/1/50.
3. Chiaberge, M.; Marconi, A. On the origin of radio loudness in active galactic nuclei and its relationship with the properties of the central supermassive black hole. *Mon. Not. R. Astron. Soc.* **2011**, *416*, 917–926. https://doi.org/10.1111/j.1365-2966.2011.19079.x.
4. Chiaberge, M.; Gilli, R.; Lotz, J.M.; Norman, C. Radio Loud AGNs are Mergers. *Astrophys. J.* **2015**, *806*, 147. https://doi.org/10.1088/0004-637X/806/2/147.
5. Narayan, R.; McClintock, J.E. Observational evidence for a correlation between jet power and black hole spin. *Mon. Not. R. Astron. Soc. Lett.* **2012**, *419*, L69–L73. https://doi.org/10.1111/j.1745-3933.2011.01181.x.
6. Garofalo, D.; Webster, B.; Bishop, K. Merger Signatures in Radio Loud and Radio Quiet Quasars. *Acta Astron.* **2020**, *70*, 75–85. https://doi.org/10.32023/0001-5237/70.1.5.
7. Garofalo, D.; North, M.; Belga, L.; Waddell, K. Why Radio Quiet Quasars are Preferred over Radio Loud Quasars Regardless of Environment and Redshift. *Astrophys. J.* **2020**, *890*, 144. https://doi.org/10.3847/1538-4357/ab6f70.
8. Waggett, P.C.; Warner, P.J.; Baldwin, J.E. NGC 6251, a very large radio galaxy with an exceptional jet. *Mon. Not. R. Astron. Soc.* **1977**, *181*, 465–474. https://doi.org/10.1093/mnras/181.3.465.
9. Blandford, R.; Meier, D.; Readhead, A. Relativistic Jets from Active Galactic Nuclei. *Annu. Rev. Astron. Astrophys.* **2019**, *57*, 467–509. https://doi.org/10.1146/annurev-astro-081817-051948.
10. Fanaroff, B.L.; Riley, J.M. The morphology of extragalactic radio sources of high and low luminosity. *Mon. Not. R. Astron. Soc.* **1974**, *167*, 31P–36P. https://doi.org/10.1093/mnras/167.1.31P.
11. Urry, C.M.; Padovani, P. Unified Schemes for Radio-Loud Active Galactic Nuclei. *Publ. Astron. Soc. Pac.* **1995**, *107*, 803. https://doi.org/10.1086/133630.
12. Ledlow, M.J.; Owen, F.N. 20 CM VLA Survey of Abell Clusters of Galaxies. VI. Radio/Optical Luminosity Functions. *Astron. J.* **1996**, *112*, 9. https://doi.org/10.1086/117985.
13. Weaver, Z.R.; Jorstad, S.G.; Marscher, A.P.; Morozova, D.A.; Troitsky, I.S.; Agudo, I.; Gómez, J.L.; Lähteenmäki, A.; Tammi, J.; Tornikoski, M. Kinematics of Parsec-Scale Jets of Gamma-Ray Bright Blazars at 43 GHz during Ten Years of the VLBA-BU-BLAZAR Program. *arXiv* **2022**, arXiv:2202.12290.
14. Prandini, E.; Ghisellini, G. The Blazar Sequence and Physical Understanding. *Galaxies* **2022**, *10*, 35
15. Feng, Q. Blazars: Time Domain. Galaxies: Special Issue "Extragalactic TeV Astronomy". 2022, unpublished.
16. Sol, H.; Zech, A. Blazar Modelling. Galaxies: Special Issue "Extragalactic TeV Astronomy". 2022, unpublished.
17. De Naurois, M. The H.E.S.S. experiment: Current status and future prospects. In Proceedings of the 36th International Cosmic Ray Conference—PoS(ICRC2019), Madison, WI, USA, 24 July–1 August 2019; Volume 358, p. 656. https://doi.org/10.22323/1.358.0656.
18. Aleksić, J.; Ansoldi, S.; Antonelli, L.A.; Antoranz, P.; Babic, A.; Bangale, P.; Barceló, M.; Barrio, J.A.; Becerra González, J.; Bednarek, W.; et al. The major upgrade of the MAGIC telescopes, Part I: The hardware improvements and the commissioning of the system. *Astropart. Phys.* **2016**, *72*, 61–75. https://doi.org/10.1016/j.astropartphys.2015.04.004.
19. Aleksić, J.; Ansoldi, S.; Antonelli, L.A.; Antoranz, P.; Babic, A.; Bangale, P.; Barceló, M.; Barrio, J.A.; Becerra González, J.; Bednarek, W.; et al. The major upgrade of the MAGIC telescopes, Part II: A performance study using observations of the Crab Nebula. *Astropart. Phys.* **2016**, *72*, 76–94. https://doi.org/10.1016/j.astropartphys.2015.02.005.
20. Holder, J. VERITAS: Status and Highlights. *Int. Cosm. Ray Conf.* **2011**, *12*, 137. https://doi.org/10.7529/ICRC2011/V12/H11.
21. Quinn, John. VERITAS: Status and Recent Results. *EPJ Web Conf.* **2019**, *209*, 01028. https://doi.org/10.1051/epjconf/201920901028.
22. Wakely, S.P.; Horan, D. TeVCat: An online catalogue for Very High Energy Gamma-Ray Astronomy. *Int. Cosm. Ray Conf.* **2008**, *3*, 1341–1344.

23. Acciari, V.A.; Aliu, E.; Arlen, T.; Aune, T.; Bautista, M.; Beilicke, M.; Benbow, W.; Boltuch, D.; Bradbury, S.M.; Buckley, J.H.; et al. VERITAS Upper Limit on the Very High Energy Emission from the Radio Galaxy NGC 1275. *Astrophys. J. Lett.* **2009**, *706*, L275–L280. https://doi.org/10.1088/0004-637X/706/2/L275.
24. Acero, F.; Aharonian, F.; Akhperjanian, A.G.; Anton, G.; Barres de Almeida, U.; Bazer-Bachi, A.R.; Becherini, Y.; Behera, B.; Bernlöhr, K.; Bochow, A.; et al. Detection of Gamma Rays from a Starburst Galaxy. *Science* **2009**, *326*, 1080. https://doi.org/10.1126/science.1178826.
25. Atwood, W.B.; Abdo, A.A.; Ackermann, M.; Althouse, W.; Anderson, B.; Axelsson, M.; Baldini, L.; Ballet, J.; Band, D.L.; Barbiellini, G.; et al. The Large Area Telescope on the Fermi Gamma-Ray Space Telescope Mission. *Astrophys. J.* **2009**, *697*, 1071–1102. https://doi.org/10.1088/0004-637X/697/2/1071.
26. CTA Consortium; Ong, R.A. The Cherenkov Telescope Array Science Goals and Current Status. *Eur. Phys. J. Web Conf.* **2019**, *209*, 01038. https://doi.org/10.1051/epjconf/201920901038.
27. Meyer, E.; Georganopoulos, M.; Lister, M.; Sparks, W.; Chiaberge, M.; Perlman, E.; Van Der Marel, R.; Anderson, J. Proper Motions of Jets on kpc Scales with HST and the VLA. *Bull. Am. Astron. Soc.* **2020**, *235*, 436.03.
28. Hall, D.N.B. *The Space Telescope Observatory: Special Session of Commission 44, IAU 18th General Assembly, Patras, Greece, August, 1982*; NASA Conference Publication: Washington, DC, USA, 1982; Volume 2244.
29. Jenkner, H. The Hubble Space Telescope Before Launch: A Personal Perspective. *Rev. Mod. Astron.* **1990**, *3*, 297–312. https://doi.org/10.1007/978-3-642-76238-3_20.
30. Burrows, C.J.; Holtzman, J.A.; Faber, S.M.; Bely, P.Y.; Hasan, H.; Lynds, C.R.; Schroeder, D. The Imaging Performance of the Hubble Space Telescope. *Astrophys. J. Lett.* **1991**, *369*, L21. https://doi.org/10.1086/185950.
31. Thompson, A.R.; Clark, B.G.; Wade, C.M.; Napier, P.J. The Very Large Array. *Astrophys. J. Suppl. Ser.* **1980**, *44*, 151–167. https://doi.org/10.1086/190688.
32. Heeschen, D.S. The Very Large Array. *Sky Telesc.* **1975**, *49*, 344.
33. Thompson, A.R.; Moran, J.M.; Swenson, G.W. *Interferometry and Synthesis in Radio Astronomy*; Springer Nature: Berlin, Germany, 2017.
34. Whitney, A.R.; Shapiro, I.I.; Rogers, A.E.E.; Robertson, D.S.; Knight, C.A.; Clark, T.A.; Goldstein, R.M.; Marandino, G.E.; Vandenberg, N.R. Quasars Revisited: Rapid Time Variations Observed via Very-Long-Baseline Interferometry. *Science* **1971**, *173*, 225–230. https://doi.org/10.1126/science.173.3993.225.
35. Rani, B. Radio Galaxies—The TeV Challenge. *Galaxies* **2019**, *7*, 23. https://doi.org/10.3390/galaxies7010023.
36. Maraschi, L.; Ghisellini, G.; Celotti, A. On the broad band energy distribution of blazars. In *Proceedings of the Multi-Wavelength Continuum Emission of AGN*; Courvoisier, T., Blecha, A., Eds.; Cambridge University Press: Cambridge, UK, 1994; Volume 159, pp. 221–232.
37. Gould, R.J. Compton and synchrotron processes in spherically-symmetric non-thermal sources. *Astron. Astrophys.* **1979**, *76*, 306–311.
38. Inoue, S.; Takahara, F. Electron Acceleration and Gamma-Ray Emission from Blazars. *Astrophys. J.* **1996**, *463*, 555. https://doi.org/10.1086/177270.
39. Lenain, J.P.; Boisson, C.; Sol, H.; Katarzyński, K. A synchrotron self-Compton scenario for the very high energy γ-ray emission of the radiogalaxy M 87. Unifying the TeV emission of blazars and other AGNs? *Astron. Astrophys.* **2008**, *478*, 111–120. https://doi.org/10.1051/0004-6361:20077995.
40. Meyer, E.T.; Fossati, G.; Georganopoulos, M.; Lister, M.L. From the Blazar Sequence to the Blazar Envelope: Revisiting the Relativistic Jet Dichotomy in Radio-loud Active Galactic Nuclei. *Astrophys. J.* **2011**, *740*, 98. https://doi.org/10.1088/0004-637X/740/2/98.
41. Ghisellini, G. The Blazar Sequence 2.0. *Galaxies* **2016**, *4*, 36. https://doi.org/10.3390/galaxies4040036.
42. Ghisellini, G.; Tavecchio, F.; Chiaberge, M. Structured jets in TeV BL Lac objects and radiogalaxies. Implications for the observed properties. *Astron. Astrophys.* **2005**, *432*, 401–410. https://doi.org/10.1051/0004-6361:20041404.
43. Keenan, M.; Meyer, E.T.; Georganopoulos, M.; Reddy, K.; French, O.J. The relativistic jet dichotomy and the end of the blazar sequence. *Mon. Not. R. Astron Soc.* **2021**, *505*, 4726–4745. https://doi.org/10.1093/mnras/stab1182.
44. Angioni, R.; Grandi, P.; Torresi, E.; Vignali, C.; Knödlseder, J. Radio galaxies with the Cherenkov Telescope Array. *Astropart. Phys.* **2017**, *92*, 42–48. https://doi.org/10.1016/j.astropartphys.2017.02.010.
45. Fermi-LAT Collaboration; Abdollahi, S.; Acero, F.; Baldini, L.; Ballet, J.; Bastieri, D.; Bellazzini, R.; Berenji, B.; Berretta, A.; Bissaldi, E.; et al. Incremental Fermi Large Area Telescope Fourth Source Catalog. *arXiv* **2022**, arXiv:2201.11184.
46. Sahakyan, N.; Yang, R.; Aharonian, F.A.; Rieger, F.M. Evidence for a Second Component in the High-energy Core Emission from Centaurus A? *Astrophys. J. Lett.* **2013**, *770*, L6. https://doi.org/10.1088/2041-8205/770/1/L6.
47. Brown, A.M.; Bœhm, C.; Graham, J.; Lacroix, T.; Chadwick, P.; Silk, J. Discovery of a new extragalactic population of energetic particles. *Phys. Rev. D* **2017**, *95*, 063018. https://doi.org/10.1103/PhysRevD.95.063018.
48. The Fermi-LAT Collaboration. Fermi Large Area Telescope Fourth Source Catalog. *arXiv* **2019**, arXiv:1902.10045.
49. Kino, M.; Wajima, K.; Kawakatu, N.; Nagai, H.; Orienti, M.; Giovannini, G.; Hada, K.; Niinuma, K.; Giroletti, M. Evidence of Jet-Clump Interaction: A Flip of the Radio Jet Head of 3C 84. *Astrophys. J.* **2018**, *864*, 118. https://doi.org/10.3847/1538-4357/aad6e3.

50. Chiaberge, M.; Celotti, A.; Capetti, A.; Ghisellini, G. Does the unification of BL Lac and FR I radio galaxies require jet velocity structures? *Astron. Astrophys.* **2000**, *358*, 104–112.
51. Müller, C.; Kadler, M.; Ojha, R.; Perucho, M.; Großberger, C.; Ros, E.; Wilms, J.; Blanchard, J.; Böck, M.; Carpenter, B.; et al. TANAMI monitoring of Centaurus A: The complex dynamics in the inner parsec of an extragalactic jet. *Astron. Astrophys.* **2014**, *569*, A115. https://doi.org/10.1051/0004-6361/201423948.
52. Böttcher, M.; Harris, D.E.; Krawczynski, H. *Relativistic Jets from Active Galactic Nuclei*; John Wiley and Sons: Hoboken, NJ, USA, 2012.
53. Mertens, F.; Lobanov, A.P.; Walker, R.C.; Hardee, P.E. Kinematics of the jet in M 87 on scales of 100–1000 Schwarzschild radii. *Astron. Astrophys.* **2016**, *595*, A54. https://doi.org/10.1051/0004-6361/201628829.
54. Walker, R.C.; Romney, J.D.; Benson, J.M. Detection of a VLBI Counterjet in NGC 1275: A Possible Probe of the Parsec-Scale Accretion Region. *Astrophys. J. Lett.* **1994**, *430*, L45. https://doi.org/10.1086/187434.
55. Gendron-Marsolais, M.; Hlavacek-Larrondo, J.; van Weeren, R.J.; Rudnick, L.; Clarke, T.E.; Sebastian, B.; Mroczkowski, T.; Fabian, A.C.; Blundell, K.M.; Sheldahl, E.; et al. High-resolution VLA low radio frequency observations of the Perseus cluster: Radio lobes, mini-halo, and bent-jet radio galaxies. *Mon. Not. R. Astron. Soc.* **2020**, *499*, 5791–5805. https://doi.org/10.1093/mnras/staa2003.
56. Ahnen, M.L.; Ansoldi, S.; Antonelli, L.A.; Arcaro, C.; Babić, A.; Banerjee, B.; Bangale, P.; Barres de Almeida, U.; Barrio, J.A.; Becerra González, J.; et al. First multi-wavelength campaign on the gamma-ray-loud active galaxy IC 310. *Astron. Astrophys.* **2017**, *603*, A25. https://doi.org/10.1051/0004-6361/201630347.
57. Baum, S.A.; O'Dea, C.P.; Giovannini, G.; Cotton, W.B.; de Koff, S.; Feretti, L.; Golombek, D.; Lara, L.; Macchetto, F.D.; Miley, G.K.; et al. HST and Merlin Observations of 3C 264–A Laboratory for Jet Physics and Unified Schemes. *Astrophys. J.* **1997**, *483*, 178–193. https://doi.org/10.1086/304221.
58. Giovannini, G.; Cotton, W.D.; Feretti, L.; Lara, L.; Venturi, T. VLBI Observations of a Complete Sample of Radio Galaxies: 10 Years Later. *Astrophys. J.* **2001**, *552*, 508–526. https://doi.org/10.1086/320581.
59. Angioni, R.; Ros, E.; Kadler, M.; Ojha, R.; Müller, C.; Edwards, P.G.; Burd, P.R.; Carpenter, B.; Dutka, M.S.; Gulyaev, S.; et al. Gamma-ray emission in radio galaxies under the VLBI scope. I. Parsec-scale jet kinematics and high-energy properties of γ-ray-detected TANAMI radio galaxies. *Astron. Astrophys.* **2019**, *627*, A148. https://doi.org/10.1051/0004-6361/201935697.
60. Fukazawa, Y.; Finke, J.; Stawarz, Ł.; Tanaka, Y.; Itoh, R.; Tokuda, S. Suzaku Observations of γ-Ray Bright Radio Galaxies: Origin of the X-ray Emission and Broadband Modeling. *Astrophys. J.* **2015**, *798*, 74. https://doi.org/10.1088/0004-637X/798/2/74.
61. Aleksić, J.; Alvarez, E.A.; Antonelli, L.A.; Antoranz, P.; Asensio, M.; Backes, M.; Barres de Almeida, U.; Barrio, J.A.; Bastieri, D.; Becerra González, J.; et al. Detection of very-high energy γ-ray emission from NGC 1275 by the MAGIC telescopes. *Astron. Astrophys.* **2012**, *539*, L2. https://doi.org/10.1051/0004-6361/201118668.
62. Benbow, W.; VERITAS Collaboration. Highlights from the VERITAS AGN Observation Program. In Proceedings of the 34th International Cosmic Ray Conference (ICRC2015), The Hague, The Netherlands, 30 July–6 August 2015; Volume 34, p. 821.
63. Jorstad, S.G.; Marscher, A.P.; Morozova, D.A.; Troitsky, I.S.; Agudo, I.; Casadio, C.; Foord, A.; Gómez, J.L.; MacDonald, N.R.; Molina, S.N.; et al. Kinematics of Parsec-scale Jets of Gamma-Ray Blazars at 43 GHz within the VLBA-BU-BLAZAR Program. *Astrophys. J.* **2017**, *846*, 98. https://doi.org/10.3847/1538-4357/aa8407.
64. Kino, M.; Niinuma, K.; Kawakatu, N.; Nagai, H.; Giovannini, G.; Orienti, M.; Wajima, K.; D'Ammando, F.; Hada, K.; Giroletti, M.; et al. Morphological Transition of the Compact Radio Lobe in 3C 84 via the Strong Jet-Cloud Collision. *Astrophys. J. Lett.* **2021**, *920*, L24. https://doi.org/10.3847/2041-8213/ac24fa.
65. Nagai, H.; Suzuki, K.; Asada, K.; Kino, M.; Kameno, S.; Doi, A.; Inoue, M.; Kataoka, J.; Bach, U.; Hirota, T.; et al. VLBI Monitoring of 3C 84 (NGC 1275) in Early Phase of the 2005 Outburst. *Publ. Astron. Soc. Jpn.* **2010**, *62*, L11. https://doi.org/10.1093/pasj/62.2.L11.
66. Nagai, H.; Haga, T.; Giovannini, G.; Doi, A.; Orienti, M.; D'Ammando, F.; Kino, M.; Nakamura, M.; Asada, K.; Hada, K.; et al. Limb-brightened Jet of 3C 84 Revealed by the 43 GHz Very-Long-Baseline-Array Observation. *Astrophys. J.* **2014**, *785*, 53. https://doi.org/10.1088/0004-637X/785/1/53.
67. Giovannini, G.; Savolainen, T.; Orienti, M.; Nakamura, M.; Nagai, H.; Kino, M.; Giroletti, M.; Hada, K.; Bruni, G.; Kovalev, Y.Y.; et al. A wide and collimated radio jet in 3C84 on the scale of a few hundred gravitational radii. *Nat. Astron.* **2018**, *2*, 472–477. https://doi.org/10.1038/s41550-018-0431-2.
68. Nagai, H.; Fujita, Y.; Nakamura, M.; Orienti, M.; Kino, M.; Asada, K.; Giovannini, G. Enhanced Polarized Emission from the One-parsec-scale Hotspot of 3C 84 as a Result of the Interaction with the Clumpy Ambient Medium. *Astrophys. J.* **2017**, *849*, 52. https://doi.org/10.3847/1538-4357/aa8e43.
69. Georganopoulos, M.; Kazanas, D. Decelerating Flows in TeV Blazars: A Resolution to the BL Lacertae-FR I Unification Problem. *Astrophys. J. Lett.* **2003**, *594*, L27–L30. https://doi.org/10.1086/378557.
70. Conselice, C.J.; Gallagher, John S., I.; Wyse, R.F.G. On the Nature of the NGC 1275 System. *Astron. J.* **2001**, *122*, 2281–2300. https://doi.org/10.1086/323534.
71. Kashiyama, K.; Mészáros, P. Galaxy Mergers as a Source of Cosmic Rays, Neutrinos, and Gamma Rays. *Astrophys. J. Lett.* **2014**, *790*, L14. https://doi.org/10.1088/2041-8205/790/1/L14.

72. Mirzoyan, R.; on behalf of the MAGIC Collaboration. ATel# 9929: MAGIC Detection of a Giant Flaring Activity from NGC 1275 at Very-High-Energy Gamma Rays. Available online: http://www.astronomerstelegram.org/?read=9929 (accessed on 12 April 2022).
73. Mukherjee, R.; for the VERITAS Collaboration. ATel# 9931: VERITAS Detection of the Radio Galaxy NGC 1275 with Elevated Very-High-Energy Gamma-Ray Emission. Available online: https://www.astronomerstelegram.org/?read=9931 (accessed on 12 April 2022).
74. MAGIC Collaboration.; Ansoldi, S.; Antonelli, L.A.; Arcaro, C.; Baack, D.; Babić, A.; Banerjee, B.; Bangale, P.; Barres de Almeida, U.; Barrio, J.A.; et al. Gamma-ray flaring activity of NGC1275 in 2016–2017 measured by MAGIC. *Astron. Astrophys.* **2018**, *617*, A91. https://doi.org/10.1051/0004-6361/201832895.
75. Harris, G.L.H.; Rejkuba, M.; Harris, W.E. The Distance to NGC 5128 (Centaurus A). *Publ. Astron. Soc. Aust.* **2010**, *27*, 457–462. https://doi.org/10.1071/AS09061.
76. Janssen, M.; Falcke, H.; Kadler, M.; Ros, E.; Wielgus, M.; Akiyama, K.; Baloković, M.; Blackburn, L.; Bouman, K.L.; Chael, A.; et al. Event Horizon Telescope observations of the jet launching and collimation in Centaurus A. *Nat. Astron.* **2021**, *5*, 1017–1028. https://doi.org/10.1038/s41550-021-01417-w.
77. Aharonian, F.; Akhperjanian, A.G.; Anton, G.; de Almeida, U.B.; Bazer-Bachi, A.R.; Becherini, Y.; Behera, B.; Benbow, W.; Bernlöhr, K.; Boisson, C.; et al. Discovery of Very High Energy γ-Ray Emission from Centaurus a with H.E.S.S. *Astrophys. J. Lett.* **2009**, *695*, L40–L44. https://doi.org/10.1088/0004-637X/695/1/L40.
78. H.E.S.S. Collaboration; Abdalla, H.; Abramowski, A.; Aharonian, F.; Ait Benkhali, F.; Angüner, E.O.; Arakawa, M.; Armand, C.; Arrieta, M.; Backes, M.; et al. The γ-ray spectrum of the core of Centaurus A as observed with H.E.S.S. and Fermi-LAT. *Astron. Astrophys.* **2018**, *619*, A71. https://doi.org/10.1051/0004-6361/201832640.
79. Rieger, F.M.; Aharonian, F.A. Centaurus A as TeV γ-ray and possible UHE cosmic ray source. *Astron. Astrophys.* **2009**, *506*, L41–L44. https://doi.org/10.1051/0004-6361/200912562.
80. Rieger, F.M. Nonthermal Processes in Black Hole-Jet Magnetospheres. *Int. J. Mod. Phys. D* **2011**, *20*, 1547–1596. https://doi.org/10.1142/S0218271811019712.
81. Kachelrieß, M.; Ostapchenko, S.; Tomàs, R. TeV Gamma Rays from Ultrahigh Energy Cosmic Ray Interactions in the Cores of Active Galactic Nuclei: Lessons from Centaurus A. *Publ. Astron. Soc. Aust.* **2010**, *27*, 482–489. https://doi.org/10.1071/AS09072.
82. Sahu, S.; Zhang, B.; Fraija, N. Hadronic-origin TeV γ rays and ultrahigh energy cosmic rays from Centaurus A. *Phys. Rev. D* **2012**, *85*, 043012. https://doi.org/10.1103/PhysRevD.85.043012.
83. Petropoulou, M.; Lefa, E.; Dimitrakoudis, S.; Mastichiadis, A. One-zone synchrotron self-Compton model for the core emission of Centaurus A revisited. *Astron. Astrophys.* **2014**, *562*, A12. https://doi.org/10.1051/0004-6361/201322833.
84. Fraija, N. Gamma-ray fluxes from the core emission of Centaurus A: A puzzle solved. *Mon. Not. R. Astron. Soc.* **2014**, *441*, 1209–1216. https://doi.org/10.1093/mnras/stu652.
85. Reynoso, M.M.; Medina, M.C.; Romero, G.E. A lepto-hadronic model for high-energy emission from FR I radiogalaxies. *Astron. Astrophys.* **2011**, *531*, A30. https://doi.org/10.1051/0004-6361/201014998.
86. Cerruti, M.; Zech, A.; Emery, G.; Guarin, D. Hadronic modeling of TeV AGN: Gammas and neutrinos. *AIP Conf. Proc.* **2017**, *1792*, 050027. https://doi.org/10.1063/1.4968973.
87. Sitarek, J.; Bednarek, W. Time-dependent gamma-ray production in the anisotropic inverse Compton $e^{+/-}$ pair cascade initiated by electrons in active galaxies. *Mon. Not. R. Astron. Soc.* **2010**, *409*, 662–678. https://doi.org/10.1111/j.1365-2966.2010.17330.x.
88. Roustazadeh, P.; Böttcher, M. Very High Energy Gamma-ray-induced Pair Cascades in the Radiation Fields of Dust Tori of Active Galactic Nuclei: Application to Cen A. *Astrophys. J.* **2011**, *728*, 134. https://doi.org/10.1088/0004-637X/728/2/134.
89. Stawarz, Ł.; Aharonian, F.; Wagner, S.; Ostrowski, M. Absorption of nuclear γ-rays on the starlight radiation in FR I sources: The case of Centaurus A. *Mon. Not. R. Astron. Soc.* **2006**, *371*, 1705–1716. https://doi.org/10.1111/j.1365-2966.2006.10807.x.
90. Hardcastle, M.J.; Croston, J.H. Modelling TeV γ-ray emission from the kiloparsec-scale jets of Centaurus A and M87. *Mon. Not. R. Astron. Soc.* **2011**, *415*, 133–142. https://doi.org/10.1111/j.1365-2966.2011.18678.x.
91. Stawarz, Ł.; Sikora, M.; Ostrowski, M. High-Energy Gamma Rays from FR I Jets. *Astrophys. J.* **2003**, *597*, 186–201. https://doi.org/10.1086/378290.
92. H.E.S.S. Collaboration; Abdalla, H.; Adam, R.; Aharonian, F.; Ait Benkhali, F.; Angüner, E.O.; Arakawa, M.; Arcaro, C.; Armand, C.; Ashkar, H.; et al. Resolving acceleration to very high energies along the jet of Centaurus A. *Nature* **2020**, *582*, 356–359. https://doi.org/10.1038/s41586-020-2354-1.
93. Bird, S.; Harris, W.E.; Blakeslee, J.P.; Flynn, C. The inner halo of M 87: A first direct view of the red-giant population. *Astron. Astrophys.* **2010**, *524*, A71. https://doi.org/10.1051/0004-6361/201014876.
94. Biretta, J.A.; Sparks, W.B.; Macchetto, F. Hubble Space Telescope Observations of Superluminal Motion in the M87 Jet. *Astrophys. J.* **1999**, *520*, 621–626. https://doi.org/10.1086/307499.
95. Biretta, J.A.; Zhou, F.; Owen, F.N. Detection of Proper Motions in the M87 Jet. *Astrophys. J.* **1995**, *447*, 582. https://doi.org/10.1086/175901.
96. Cheung, C.C.; Harris, D.E.; Stawarz, Ł. Superluminal Radio Features in the M87 Jet and the Site of Flaring TeV Gamma-ray Emission. *Astrophys. J. Lett.* **2007**, *663*, L65–L68. https://doi.org/10.1086/520510.
97. Giroletti, M.; Hada, K.; Giovannini, G.; Casadio, C.; Beilicke, M.; Cesarini, A.; Cheung, C.C.; Doi, A.; Krawczynski, H.; Kino, M.; et al. The kinematic of HST-1 in the jet of M 87. *Astron. Astrophys.* **2012**, *538*, L10. https://doi.org/10.1051/0004-6361/201218794.

98. Kovalev, Y.Y.; Lister, M.L.; Homan, D.C.; Kellermann, K.I. The Inner Jet of the Radio Galaxy M87. *Astrophys. J. Lett.* **2007**, *668*, L27–L30. https://doi.org/10.1086/522603.
99. Asada, K.; Nakamura, M.; Doi, A.; Nagai, H.; Inoue, M. Discovery of Sub- to Superluminal Motions in the M87 Jet: An Implication of Acceleration from Sub-relativistic to Relativistic Speeds. *Astrophys. J. Lett.* **2014**, *781*, L2. https://doi.org/10.1088/2041-8205/781/1/L2.
100. Lebohec, S.; VERITAS Collaboration. Observations of M87 and Mkn40 at energies E > 300 GeV. In Proceedings of the International Cosmic Ray Conference, Hamburg, Germany, 7–15 August 2001; Volume 7, p. 2643.
101. Aharonian, F.; Akhperjanian, A.; Beilicke, M.; Bernlöhr, K.; Börst, H.G.; Bojahr, H.; Bolz, O.; Coarasa, T.; Contreras, J.L.; Cortina, J.; et al. Is the giant radio galaxy M 87 a TeV gamma-ray emitter? *Astron. Astrophys.* **2003**, *403*, L1–L5. https://doi.org/10.1051/0004-6361:20030372.
102. Daum, A.; Hermann, G.; Heß, M.; Hofmann, W.; Lampeitl, H.; Pühlhofer, G.; Aharonian, F.; Akhperjanian, A.G.; Barrio, J.A.; Beglarian, A.S.; et al. First results on the performance of the HEGRA IACT array. *Astropart. Phys.* **1997**, *8*, 1–11. https://doi.org/10.1016/S0927-6505(97)00031-5.
103. Aharonian, F.; Akhperjanian, A.G.; Bazer-Bachi, A.R.; Beilicke, M.; Benbow, W.; Berge, D.; Bernlöhr, K.; Boisson, C.; Bolz, O.; Borrel, V.; et al. Fast Variability of Tera-Electron Volt γ Rays from the Radio Galaxy M87. *Science* **2006**, *314*, 1424–1427. https://doi.org/10.1126/science.1134408.
104. Acciari, V.A.; Beilicke, M.; Blaylock, G.; Bradbury, S.M.; Buckley, J.H.; Bugaev, V.; Butt, Y.; Celik, O.; Cesarini, A.; Ciupik, L.; et al. Observation of Gamma-Ray Emission from the Galaxy M87 above 250 GeV with VERITAS. *Astrophys. J.* **2008**, *679*, 397–403. https://doi.org/10.1086/587458.
105. Albert, J.; Aliu, E.; Anderhub, H.; Antonelli, L.A.; Antoranz, P.; Backes, M.; Baixeras, C.; Barrio, J.A.; Bartko, H.; Bastieri, D.; et al. Very High Energy Gamma-ray Observations of Strong Flaring Activity in M87 in 2008 February. *Astrophys. J. Lett.* **2008**, *685*, L23. https://doi.org/10.1086/592348.
106. Abramowski, A.; Acero, F.; Aharonian, F.; Akhperjanian, A.G.; Anton, G.; Balzer, A.; Barnacka, A.; Barres de Almeida, U.; Becherini, Y.; Becker, J.; et al. The 2010 Very High Energy γ-ray Flare and 10 Years of Multi-wavelength Observations of M 87. *Astrophys. J.* **2012**, *746*, 151. https://doi.org/10.1088/0004-637X/746/2/151.
107. National Radio Astronomy Observatory. Multi-Wavelength Observations Reveal Impact of Black Hole on M87 Galaxy. Available online: https://public.nrao.edu/news/m87-black-hole-multi-wavelength-eht/ (accessed on 12 April 2022).
108. Perlman, E.S.; Padgett, C.A.; Georganopoulos, M.; Worrall, D.M.; Kastner, J.H.; Franz, G.; Birkinshaw, M.; Dulwich, F.; O'Dea, C.P.; Baum, S.A.; et al. A Multi-Wavelength Spectral and Polarimetric Study of the Jet of 3C 264. *Astrophys. J.* **2010**, *708*, 171–187. https://doi.org/10.1088/0004-637X/708/1/171.
109. Archer, A.; Benbow, W.; Bird, R.; Brill, A.; Buchovecky, M.; Buckley, J.H.; Carini, M.T.; Christiansen, J.L.; Chromey, A.J.; Daniel, M.K.; et al. VERITAS Discovery of VHE Emission from the Radio Galaxy 3C 264: A Multiwavelength Study. *Astrophys. J.* **2020**, *896*, 41. https://doi.org/10.3847/1538-4357/ab910e.
110. Lara, L.; Feretti, L.; Giovannini, G.; Baum, S.; Cotton, W.D.; O'Dea, C.P.; Venturi, T. The Radio-Optical Jet in NGC 3862 from Parsec to Subkiloparsec Scales. *Astrophys. J.* **1999**, *513*, 197–206. https://doi.org/10.1086/306852.
111. Boccardi, B.; Migliori, G.; Grandi, P.; Torresi, E.; Mertens, F.; Karamanavis, V.; Angioni, R.; Vignali, C. The TeV-emitting radio galaxy 3C 264. VLBI kinematics and SED modeling. *Astron. Astrophys.* **2019**, *627*, A89. https://doi.org/10.1051/0004-6361/201935183.
112. Meyer, E.T.; Georganopoulos, M.; Sparks, W.B.; Perlman, E.; van der Marel, R.P.; Anderson, J.; Sohn, S.T.; Biretta, J.; Norman, C.; Chiaberge, M. A kiloparsec-scale internal shock collision in the jet of a nearby radio galaxy. *Nature* **2015**, *521*, 495–497. https://doi.org/10.1038/nature14481.
113. Rulten, C.B.; Brown, A.M.; Chadwick, P.M. A search for Centaurus A-like features in the spectra of Fermi-LAT detected radio galaxies. *Mon. Not. R. Astron. Soc.* **2020**, *492*, 4666–4679. https://doi.org/10.1093/mnras/staa054.
114. Dyrda, M.; Wierzcholska, A.; Moderski, R.; Ostrowski, M.; Stawarz, L. Discovery of VHE gamma-rays from the radio galaxy PKS 0625-354 with H.E.S.S. In Proceedings of the 34th International Cosmic ray Conference (ICRC2015), The Hague, The Netherlands, 30 July–6 August 2015; Volume 34, p. 801.
115. Ekers, R.D.; Wall, J.V.; Shaver, P.A.; Goss, W.M.; Fosbury, R.A.E.; Danziger, I.J.; Moorwood, A.F.M.; Malin, D.F.; Monk, A.S.; Ekers, J.A. A complete sample of radio galaxies—I. The radio data. *Mon. Not. R. Astron. Soc.* **1989**, *236*, 737–777. https://doi.org/10.1093/mnras/236.4.737.
116. Venturi, T.; Morganti, R.; Tzioumis, T.; Reynolds, J. Parsec-scale structures of radio galaxies in the 2-Jy sample. *Astron. Astrophys.* **2000**, *363*, 84–92.
117. Ojha, R.; Kadler, M.; Böck, M.; Booth, R.; Dutka, M.S.; Edwards, P.G.; Fey, A.L.; Fuhrmann, L.; Gaume, R.A.; Hase, H.; et al. TANAMI: Tracking active galactic nuclei with austral milliarcsecond interferometry. I. First-epoch 8.4 GHz images. *Astron. Astrophys.* **2010**, *519*, A45. https://doi.org/10.1051/0004-6361/200912724.
118. Wills, K.A.; Morganti, R.; Tadhunter, C.N.; Robinson, T.G.; Villar-Martin, M. Emission lines and optical continuum in low-luminosity radio galaxies. *Mon. Not. R. Astron. Soc.* **2004**, *347*, 771–786. https://doi.org/10.1111/j.1365-2966.2004.07195.x.
119. H. E. S. S. Collaboration; Abdalla, H.; Abramowski, A.; Aharonian, F.; Ait Benkhali, F.; Akhperjanian, A.G.; Andersson, T.; Angüner, E.O.; Arrieta, M.; Aubert, P.; et al. H.E.S.S. discovery of very high energy γ-ray emission from PKS 0625-354. *Mon. Not. R. Astron. Soc.* **2018**, *476*, 4187–4198. https://doi.org/10.1093/mnras/sty439.

120. Mariotti, M.; MAGIC Collaboration. Discovery of Very High Energy Gamma-ray Emission from NGC1275 by MAGIC. *Astron. Telegr.* **2010**, *2916*.
121. Aleksić, J.; Antonelli, L.A.; Antoranz, P.; Backes, M.; Barrio, J.A.; Bastieri, D.; Becerra González, J.; Bednarek, W.; Berdyugin, A.; Berger, K.; et al. Detection of Very High Energy γ-ray Emission from the Perseus Cluster Head-Tail Galaxy IC 310 by the MAGIC Telescopes. *Astrophys. J. Lett.* **2010**, *723*, L207–L212. https://doi.org/10.1088/2041-8205/723/2/L207.
122. Graham, J.A.; Brown, A.M.; Chadwick, P.M. Fermi-LAT observations of extreme spectral variability in IC 310. *Mon. Not. R. Astron. Soc.* **2019**, *485*, 3277–3287. https://doi.org/10.1093/mnras/stz588.
123. Kadler, M.; Eisenacher, D.; Ros, E.; Mannheim, K.; Elsässer, D.; Bach, U. The blazar-like radio structure of the TeV source IC 310. *Astron. Astrophys.* **2012**, *538*, L1. https://doi.org/10.1051/0004-6361/201118212.
124. Atkins, R.; Benbow, W.; Berley, D.; Blaufuss, E.; Bussons, J.; Coyne, D.G.; Delay, R.S.; De Young, T.; Dingus, B.L.; Dorfan, D.E.; et al. Observation of TeV Gamma Rays from the Crab Nebula with Milagro Using a New Background Rejection Technique. *Astrophys. J.* **2003**, *595*, 803–811. https://doi.org/10.1086/377498.
125. Atkins, R.; Benbow, W.; Berley, D.; Blaufuss, E.; Bussons, J.; Coyne, D.G.; De Young, T.; Dingus, B.L.; Dorfan, D.E.; Ellsworth, R.W.; et al. TeV Gamma-Ray Survey of the Northern Hemisphere Sky Using the Milagro Observatory. *Astrophys. J.* **2004**, *608*, 680–685. https://doi.org/10.1086/420880.
126. ARGO-YBJ Collaboration.; Bacci, C.; Bao, K.Z.; Barone, F.; Bartoli, B.; Bernardini, P.; Bussino, S.; Calloni, E.; Cao, B.Y.; Cardarelli, R.; et al. Results from the ARGO-YBJ test experiment. *Astropart. Phys.* **2002**, *17*, 151–165.
127. Abeysekara, A.U.; Albert, A.; Alfaro, R.; Alvarez, C.; Álvarez, J.D.; Arceo, R.; Arteaga-Velázquez, J.C.; Ayala Solares, H.A.; Barber, A.S.; Baughman, B.; et al. The 2HWC HAWC Observatory Gamma-Ray Catalog. *Astrophys. J.* **2017**, *843*, 40. https://doi.org/10.3847/1538-4357/aa7556.
128. Di Sciascio, G. The LHAASO experiment: From Gamma-Ray Astronomy to Cosmic Rays. *Nuclear Part. Phys. Proc.* **2016**, *279–281*, 166–173. https://doi.org/10.1016/j.nuclphysbps.2016.10.024.
129. Albert, A.; Alfaro, R.; Ashkar, H.; Alvarez, C.; Álvarez, J.; Arteaga-Velázquez, J.C.; Ayala Solares, H.A.; Arceo, R.; Bellido, J.A.; BenZvi, S.; et al. Science Case for a Wide Field-of-View Very-High-Energy Gamma-ray Observatory in the Southern Hemisphere. *arXiv* **2019**, arXiv:1902.08429.
130. Albert, A.; Alvarez, C.; Angeles Camacho, J.R.; Arteaga-Velázquez, J.C.; Arunbabu, K.P.; Avila Rojas, D.; Ayala Solares, H.A.; Baghmanyan, V.; Belmont-Moreno, E.; BenZvi, S.Y.; et al. A Survey of Active Galaxies at TeV Photon Energies with the HAWC Gamma-Ray Observatory. *Astrophys. J.* **2021**, *907*, 67. https://doi.org/10.3847/1538-4357/abca9a.
131. Vernetto, S.; LHAASO Collaboration. Gamma Ray Astronomy with LHAASO. *J. Phys. Conf. Ser.* **2016**, *718*, 052043. https://doi.org/10.1088/1742-6596/718/5/052043.
132. Garofalo, D.; Singh, C.B.; Zack, A. The distribution and lifetime of powerful radio galaxies as a function of environment and redshift. *Sci. Rep.* **2018**, *8*, 15097. https://doi.org/10.1038/s41598-018-33532-6.
133. Williams, W.L.; Calistro Rivera, G.; Best, P.N.; Hardcastle, M.J.; Röttgering, H.J.A.; Duncan, K.J.; de Gasperin, F.; Jarvis, M.J.; Miley, G.K.; Mahony, E.K.; et al. LOFAR-Boötes: Properties of high- and low-excitation radio galaxies at $0.5 < z < 2.0$. *Mon. Not. R. Astron Soc.* **2018**, *475*, 3429–3452. https://doi.org/10.1093/mnras/sty026.
134. Padovani, P.; Urry, C.M. Fanaroff–Riley I Galaxies as the Parent Population of BL Lacertae Objects. I. X-ray Constraints. *Astrophys. J.* **1990**, *356*, 75. https://doi.org/10.1086/168817.
135. Lister, M.L.; Aller, M.F.; Aller, H.D.; Hodge, M.A.; Homan, D.C.; Kovalev, Y.Y.; Pushkarev, A.B.; Savolainen, T. MOJAVE. XV. VLBA 15 GHz Total Intensity and Polarization Maps of 437 Parsec-scale AGN Jets from 1996 to 2017. *Astrophys. J. Suppl. Ser.* **2018**, *234*, 12. https://doi.org/10.3847/1538-4365/aa9c44.
136. Jorstad, S.; Marscher, A. The VLBA-BU-BLAZAR Multi-Wavelength Monitoring Program. *Galaxies* **2016**, *4*, 47. https://doi.org/10.3390/galaxies4040047.
137. Gardner, J.P.; Mather, J.C.; Clampin, M.; Doyon, R.; Greenhouse, M.A.; Hammel, H.B.; Hutchings, J.B.; Jakobsen, P.; Lilly, S.J.; Long, K.S.; et al. The James Webb Space Telescope. *Space Sci. Rev.* **2006**, *123*, 485–606. https://doi.org/10.1007/s11214-006-8315-7.
138. Braun, R.; Bourke, T.; Green, J.A.; Keane, E.; Wagg, J. Advancing Astrophysics with the Square Kilometre Array. In Proceedings of the Advancing Astrophysics with the Square Kilometre Array (AASKA14), Giardini Naxos, Italy, 9–13 June 2014; p. 174.
139. Lister, M.L.; Kellermann, K.I.; Kharb, P. High-resolution Imaging of Radio Jets Launched by Active Galactic Nuclei: New Insights on Formation, Structure, and Evolution Enabled by the ngVLA. Sci. Next Gener. Very Large Array **2018**, *517*, 619.
140. Weisskopf, M.C.; Brinkman, B.; Canizares, C.; Garmire, G.; Murray, S.; Van Speybroeck, L.P. An Overview of the Performance and Scientific Results from the Chandra X-ray Observatory. *Publ. Astron. Soc. Pac.* **2002**, *114*, 1–24. https://doi.org/10.1086/338108.
141. Abdo, A.A.; Ackermann, M.; Ajello, M.; Atwood, W.B.; Baldini, L.; Ballet, J.; Barbiellini, G.; Bastieri, D.; Baughman, B.M.; Bechtol, K.; et al. Fermi Gamma-Ray Imaging of a Radio Galaxy. *Science* **2010**, *328*, 725. https://doi.org/10.1126/science.1184656.
142. Ait Benkhali, F.; Chakraborty, N.; Rieger, F.M. Complex gamma-ray behavior of the radio galaxy M 87. *Astron. Astrophys.* **2019**, *623*, A2. https://doi.org/10.1051/0004-6361/201732334.
143. Baghmanyan, V.; Gasparyan, S.; Sahakyan, N. Rapid Gamma-ray Variability of NGC 1275. *Astrophys. J.* **2017**, *848*, 111. https://doi.org/10.3847/1538-4357/aa8c7b.
144. Chiaberge, M.; Capetti, A.; Celotti, A. The BL Lac heart of Centaurus A. *Mon. Not. R. Astron. Soc.* **2001**, *324*, L33–L37. https://doi.org/10.1046/j.1365-8711.2001.04642.x.

145. Abdo, A.A.; Ackermann, M.; Ajello, M.; Atwood, W.B.; Baldini, L.; Ballet, J.; Barbiellini, G.; Bastieri, D.; Baughman, B.M.; Bechtol, K.; et al. Fermi Large Area Telescope View of the Core of the Radio Galaxy Centaurus A. *Astrophys. J.* **2010**, *719*, 1433–1444. https://doi.org/10.1088/0004-637X/719/2/1433.
146. Giannios, D.; Uzdensky, D.A.; Begelman, M.C. Fast TeV variability in blazars: Jets in a jet. *Mon. Not. R. Astron. Soc. Lett.* **2009**, *395*, L29–L33. https://doi.org/10.1111/j.1745-3933.2009.00635.x.
147. Aleksić, J.; Ansoldi, S.; Antonelli, L.A.; Antoranz, P.; Babic, A.; Bangale, P.; Barrio, J.A.; González, J.B.; Bednarek, W.; Bernardini, E.; et al. Black hole lightning due to particle acceleration at subhorizon scales. *Science* **2014**, *346*, 1080–1084. https://doi.org/10.1126/science.1256183.
148. Rieger, F.; Levinson, A. Radio Galaxies at VHE Energies. *Galaxies* **2018**, *6*, 116. https://doi.org/10.3390/galaxies6040116.
149. Hillas, A.M. Cosmic Rays: Recent Progress and some Current Questions. *arXiv* **2006**, arXiv:ph/0607109.
150. Castellina, A. Highlights from the Pierre Auger Observatory and prospects for AugerPrime. In Proceedings of the 36th International Cosmic Ray Conference (ICRC2019), Madison, WI, USA, 24 July–1 August 2019; Volume 36, p. 4.
151. Pierre Auger Collaboration.; Abraham, J.; Abreu, P.; Aglietta, M.; Aguirre, C.; Allard, D.; Allekotte, I.; Allen, J.; Allison, P.; Alvarez, C.; et al. Correlation of the Highest-Energy Cosmic Rays with Nearby Extragalactic Objects. *Science* **2007**, *318*, 938. https://doi.org/10.1126/science.1151124.
152. Pierre Auger Collaboration.; Abraham, J.; Abreu, P.; Aglietta, M.; Aguirre, C.; Allard, D.; Allekotte, I.; Allen, J.; Allison, P.; Alvarez-Muñiz, J.; et al. Correlation of the highest-energy cosmic rays with the positions of nearby active galactic nuclei. *Astropart. Phys.* **2008**, *29*, 188–204. https://doi.org/10.1016/j.astropartphys.2008.01.002.
153. Cuoco, A.; Hannestad, S. Ultrahigh energy neutrinos from Centaurus A and the Auger hot spot. *Phys. Rev. D* **2008**, *78*, 023007. https://doi.org/10.1103/PhysRevD.78.023007.
154. Kachelrieß, M.; Ostapchenko, S.; Tomàs, R. High energy radiation from Centaurus A. *New J. Phys.* **2009**, *11*, 065017. https://doi.org/10.1088/1367-2630/11/6/065017.
155. Koers, H.B.J.; Tinyakov, P. Relation between the neutrino flux from Centaurus A and the associated diffuse neutrino flux. *Phys. Rev. D* **2008**, *78*, 083009. https://doi.org/10.1103/PhysRevD.78.083009.
156. Becker Tjus, J.; Eichmann, B.; Halzen, F.; Kheirandish, A.; Saba, S.M. High-energy neutrinos from radio galaxies. *Phys. Rev. D* **2014**, *89*, 123005. https://doi.org/10.1103/PhysRevD.89.123005.
157. Hooper, D. A case for radio galaxies as the sources of IceCube's astrophysical neutrino flux. *J. Cosmol. Astropart. Phys.* **2016**, *2016*, 002. https://doi.org/10.1088/1475-7516/2016/09/002.
158. Fraija, N.; Marinelli, A. Neutrino, γ-Ray, and Cosmic-Ray Fluxes from the Core of the Closest Radio Galaxies. *Astrophys. J.* **2016**, *830*, 81. https://doi.org/10.3847/0004-637X/830/2/81.
159. Blanco, C.; Hooper, D. High-energy gamma rays and neutrinos from nearby radio galaxies. *J. Cosmol. Astropart. Phys.* **2017**, *2017*, 017. https://doi.org/10.1088/1475-7516/2017/12/017.
160. Tavecchio, F.; Righi, C.; Capetti, A.; Grandi, P.; Ghisellini, G. High-energy neutrinos from FR0 radio galaxies? *Mon. Not. R. Astron. Soc.* **2018**, *475*, 5529–5534. https://doi.org/10.1093/mnras/sty251.
161. Baldi, R.D.; Capetti, A.; Giovannini, G. Pilot study of the radio-emitting AGN population: The emerging new class of FR 0 radio-galaxies. *Astron. Astrophys.* **2015**, *576*, A38. https://doi.org/10.1051/0004-6361/201425426.
162. Baldi, R.D.; Capetti, A.; Giovannini, G. High-resolution VLA observations of FR0 radio galaxies: The properties and nature of compact radio sources. *Mon. Not. R. Astron. Soc.* **2019**, *482*, 2294–2304. https://doi.org/10.1093/mnras/sty2703.
163. Baldi, R.D.; Torresi, E.; Migliori, G.; Balmaverde, B. The High Energy View of FR0 Radio Galaxies. *Galaxies* **2019**, *7*, 76. https://doi.org/10.3390/galaxies7030076.
164. Plavin, A.; Kovalev, Y.Y.; Kovalev, Y.A.; Troitsky, S. Observational Evidence for the Origin of High-energy Neutrinos in Parsec-scale Nuclei of Radio-bright Active Galaxies. *Astrophys. J.* **2020**, *894*, 101. https://doi.org/10.3847/1538-4357/ab86bd.
165. Fraija, N.; Marinelli, A.; Galván-Gámez, A.; Aguilar-Ruiz, E. Modeling the spectral energy distribution of the radio galaxy IC310. *Astropart. Phys.* **2017**, *89*, 14–22. https://doi.org/10.1016/j.astropartphys.2017.01.001.
166. EHT MWL Science Working Group; Algaba, J.C.; Anczarski, J.; Asada, K.; Baloković, M.; Chandra, S.; Cui, Y.Z.; Falcone, A.D.; Giroletti, M.; Goddi, C.; et al. Broadband Multi-wavelength Properties of M87 during the 2017 Event Horizon Telescope Campaign. *Astrophys. J. Lett.* **2021**, *911*, L11. https://doi.org/10.3847/2041-8213/abef71.
167. Bignall, H.E.; Croft, S.; Hovatta, T.; Koay, J.Y.; Lazio, J.; Macquart, J.P.; Reynolds, C. Time domain studies of Active Galactic Nuclei with the Square Kilometre Array. In Proceedings of the Advancing Astrophysics with the Square Kilometre Array (AASKA14), Giardini Naxos, Italy, 9–13 June 2014; p. 58.
168. Giroletti, M.; Orienti, M.; D'Ammando, F.; Massaro, F.; Tosti, G.; LICO, R.; Giovannini, G.; Agudo, I.; Alberdi, A.; Bignall, H.E.; et al. The connection between radio and high energy emission in black hole powered systems in the SKA era. In Proceedings of the Advancing Astrophysics with the Square Kilometre Array (AASKA14), Giardini Naxos, Italy, 9–13 June 2014; p. 153.
169. Garrington, S.T.; Anderson, B.; Baines, C.; Battilana, J.A.; Bentley, M.N.; Brown, D.; Burgess, P.; Diamond, P.J.; Kitching, G.J.; McCool, R.; et al. e-MERLIN. In *Proceedings of the Ground-Based Telescopes*; International Society for Optics and Photonics; SPIE: Washington, DC, USA, 2004; Volume 5489, pp. 332–343.https://doi.org/10.1117/12.553235.
170. Paragi, Z.; Godfrey, L.; Reynolds, C.; Rioja, M.J.; Deller, A.; Zhang, B.; Gurvits, L.; Bietenholz, M.; Szomoru, A.; Bignall, H.E.; et al. Very Long Baseline Interferometry with the SKA. In Proceedings of the Advancing Astrophysics with the Square Kilometre Array (AASKA14), Giardini Naxos, Italy, 29 May 2015; p. 143.